Ground Gain in Theory and Practice

By Gaëtan Horlin, ON4KHG

Contents

1. Introduction

The development of digital modes has opened the doors of EME (Earth-Moon-Earth) communications to small stations, compared with the standards of equipment previously required for CW moonbounce. Even more, it revealed the CW EME capabilities of these small stations, many of them having no antenna elevation system (as in my case). All this can be achieved or, at least helped, thanks to the so-called "Ground Gain".

Ground Gain has been emphasized by the 144 MHz EME community, but it is also of prime interest for the terrestrial propagation modes. Indeed, we will see below that if the free space antenna gain of a station is an important parameter, the environment surrounding the antenna is as much important, if not even more.

Apart the well known article of Palle, OZ1RH [1a] about the Ground Gain (focusing on tropo-scatter), there has not been a lot of articles on that topic in the amateur literature.

This article, focusing on 144 MHz band, is the result of researches in the literature and own experiments. It has been published in the German magazine "**DUBUS**" (in English and German languages), issue 3/2011.

2. Ground Reflection Geometry

2.1. Flat Ground
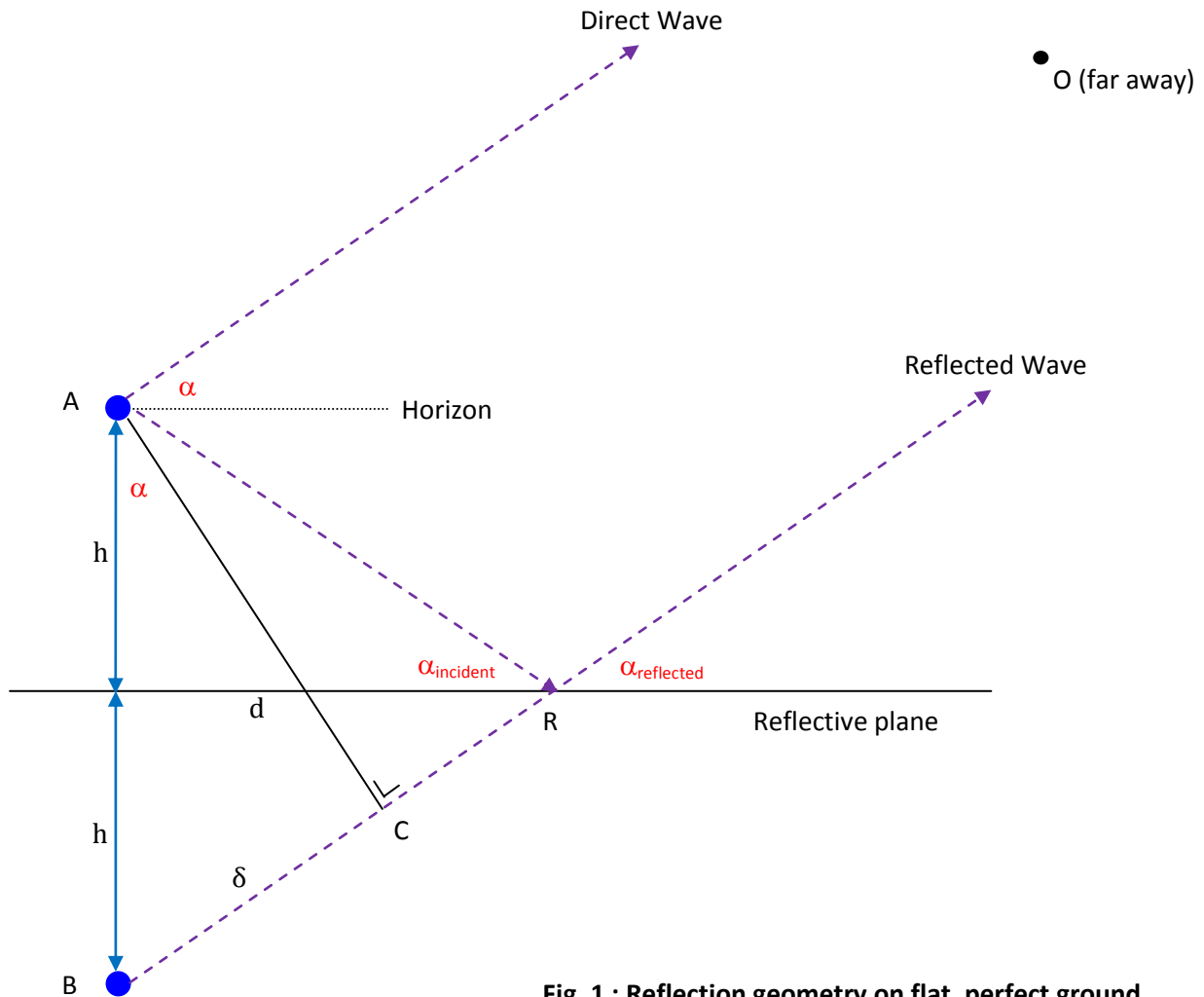
Fig. 1 : Reflection geometry on flat, perfect ground

If we locate an isotropic antenna (equally radiating in all directions) at A, over a perfectly flat reflective plane surface (conductor), the wave front radiated by the antenna will hit the reflective plane and will be reflected with the same angle as the incidence angle. This is the "reflection law" :

$$\alpha_{\text{reflected}} = \alpha_{\text{incident}} = \alpha$$

Seen from "far away enough" from the antenna, the direct and reflected rays are assumed to be parallel. From this far observation point, which we will call "O", the reflected ray appears to originate from a second antenna, located at B, equally distant from the reflective plane than the source antenna, A. The antenna located at B is called the "image antenna". This is of course a pure theoretical concept.

As the segment |AC| is perpendicular to the reflected ray, the paths |AO| and |CO| have the same length. So, if the reflected ray would be originating from C, the direct and reflected waves would have the same phase and the electric field would be doubled at O, compared to the single direct wave. However, the reflected wave is actually not originating from C but from B and the segment |BC| is introducing an extra path length δ, so that at O, the direct and reflected waves are not necessarily in phase anymore. If α, the elevation angle, varies, δ will also vary so that for certain elevation angles, the direct and reflected waves will

be in-phase at O (the electric field is doubled) or out-of-phase, leading to the cancellation of the two waves (the electric field equals to zero) ; we have respectively constructive and destructive interference.

In the right-angled triangle ABC : $\delta = 2 * h * \sin(\alpha)$

The distance d (in m) between the antenna and the reflection point (R) is given by :

$$d = \frac{h}{\tan(\alpha)}$$

α : elevation angle [°]
h : antenna height [m]
δ : extra path length [m]
d : distance between the antenna and the reflection point [m]

2.2.   Tilted Ground

If we assess now what is going on over a downward sloping ground in front of the antenna, we come up with the following picture (Fig. 2).
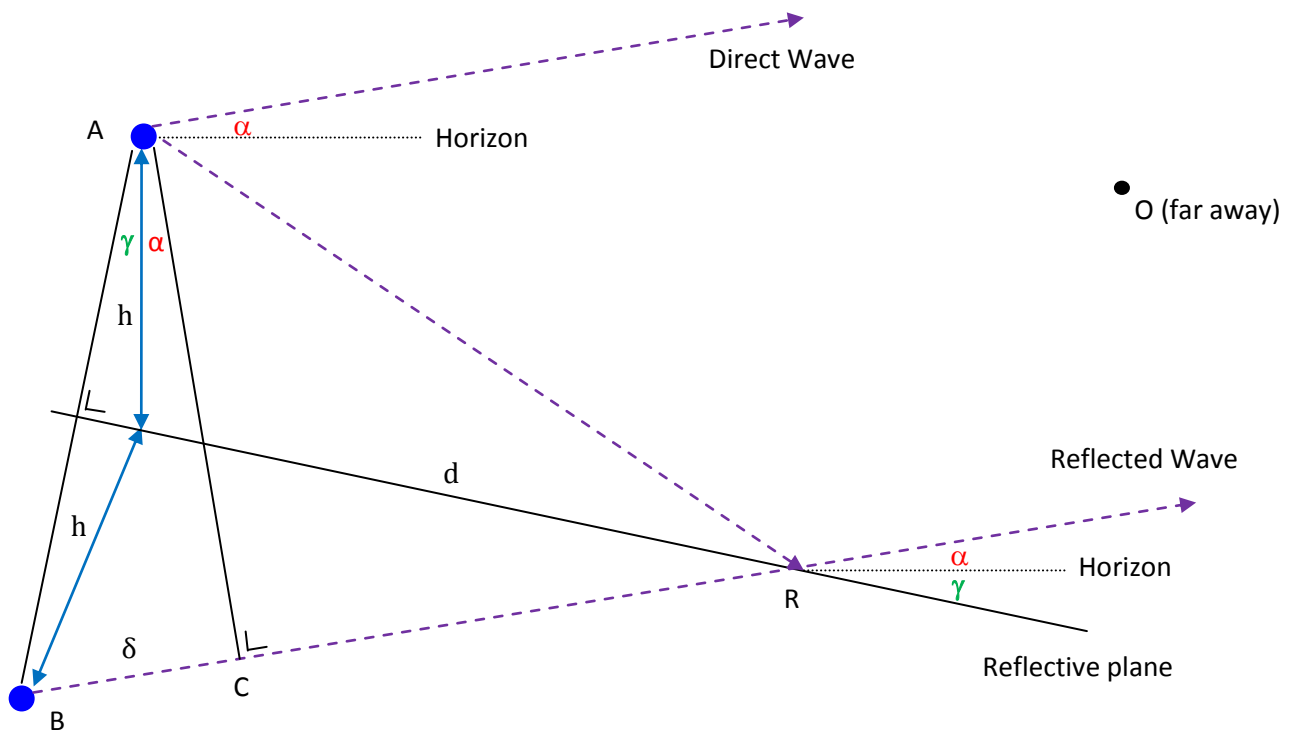
Fig. 2 : Reflection geometry on flat tilted, perfect ground

In this case : $\delta = 2 * h * \cos(\alpha) * \sin(\alpha - \gamma)$

And :

$$d = h * \left[\frac{\cos(\gamma)}{\tan(\alpha - \gamma)} - \sin(\gamma) \right]$$

γ : downward slope tilt angle [°]

3. Perfectly Reflective Ground Plane

3.1. Boundary Conditions

The Maxwell equations define the "boundary conditions" at the reflective plane which separates the two media containing the antenna A and its image B. If the boundary is a perfectly conducting surface, as assumed here, the sum of all the tangential (horizontal) electric fields (E_t) equals to zero, as shown in Fig. 3a. This means that the electric field radiated by the image (B) of the horizontally polarized antenna is in phase opposition (180° phase shift) to the one radiated by the source antenna (A).

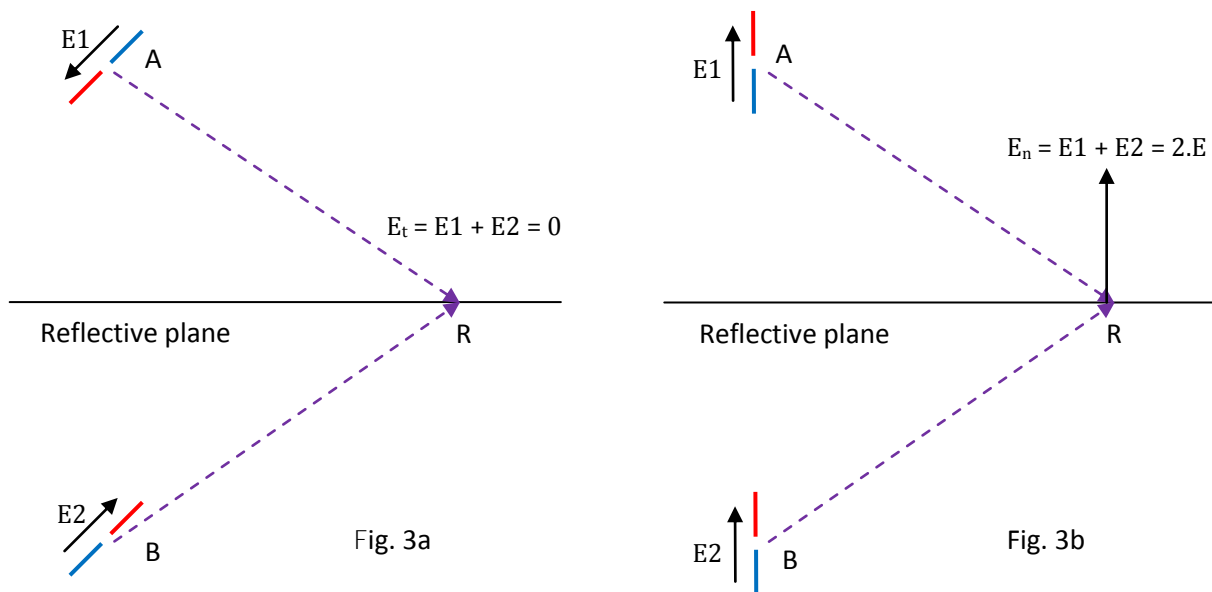**Fig. 3 : Boundary conditions for (a) horizontal and (b) vertical polarization**

E = electric field
E_t = tangential (horizontal) component of the electric field
E_n = normal (perpendicular to the reflective plane) component of the electric field

What happens for vertical polarizations is depicted above in Fig. 3b. The wave front generated by a vertically polarized antenna does not suffer any phase shift when reflected by a flat and perfectly conducting surface, while (as seen above) the same surface reflecting a horizontally polarized wave front yields to a 180° phase shift. This means that the elevation radiation patterns for horizontally and vertically polarized antennas over ground will be different.

The field pattern generated by a source antenna (A) located above a perfectly conducting surface is the same as if this conducting surface is removed and replaced by the image antenna (B). So, the field pattern of a source antenna above the ground equals to the field pattern of the source antenna plus its image in free space. Now, coming back to the case under investigation, we have a phase shift due to the extra path δ and, either no extra phase shift or a 180° phase shift, depending on the polarization. Let's call Δ the total phase shift.

For vertical polarization :

$$\Delta = \delta[°] = \frac{\delta[m]}{\lambda} * 360°$$

For horizontal polarization :

$$\Delta = \delta[°] + 180° = \left(\frac{\delta[m]}{\lambda} * 360°\right) + 180°$$

Δ : total phase shift [°]

$$\lambda[m] = \frac{300}{f\,[MHz]}$$

3.2. Magnitude and Geometry of the Antenna Lobes

In this section, as well as in section 4, we will deal with complex numbers which we will use in a number of different but always equivalent forms :

- Cartesian or rectangular form : $\mathbf{z} = a + j * b$
- Polar form : $\mathbf{z} = |z| * e^{j\theta}$
- Trigonometric form : $\mathbf{z} = |z| * \big(\cos(\theta) + j * \sin(\theta)\big)$

The real part and the imaginary part of the complex number $\mathbf{z}$ in its Cartesian form are respectively a and b. In the equivalent polar or trigonometric forms, $|z|$ is the modulus (magnitude) and θ is the argument (phase). Complete complex numbers such as $\mathbf{z}$ will be written in bold characters.

To convert one form into one of the others, one will use the formulas below :

Cartesian ➜ polar or trigonometric :

$$|z| = \sqrt{a^2 + b^2}$$
$$\theta = \arctan\left(\frac{b}{a}\right)$$

Polar or trigonometric ➜ Cartesian :

$$a = |z| * \cos(\theta)$$
$$b = |z| * \sin(\theta)$$

Coming back to the pictures of section 2, as viewed from far away from the antenna, if we assume that the extra path length encountered by the reflected wave compared to the direct wave (i.e. |AR|-|CR|) introduces a negligible attenuation and we continue to assume a perfect (non-lossy) reflection, we can write the mathematical expression of the electric field originating from the source antenna (reference magnitude = 1 and reference phase = 0) :

$$\mathbf{E_{direct}} = 1 * e^{j0} = 1 + j * 0$$

And for the field originating from the image antenna :

$$\mathbf{E_{reflected}} = 1 * e^{j\Delta} = \cos(\Delta) + j * \sin(\Delta)$$

The total field is :

$$\mathbf{E} = \mathbf{E_{direct}} + \mathbf{E_{reflected}} = \big(1 + \cos(\Delta)\big) + j * \sin(\Delta)$$

The magnitude or modulus of E is :

$$|E| = \sqrt{\big(1 + \cos(\Delta)\big)^2 + (\sin(\Delta))^2} = \sqrt{2 * \big(1 + \cos(\Delta)\big)} = \sqrt{2} * \sqrt{\big(1 + \cos(\Delta)\big)}$$

If we substitute Δ by its expression in function of δ, respectively for vertical and horizontal polarizations (see section 3.1.) and if we calculate |E| for α (elevation angle) varying from 0° to 60°, with h (antenna height) being 17 m above the "ground" level, we get the following graph :
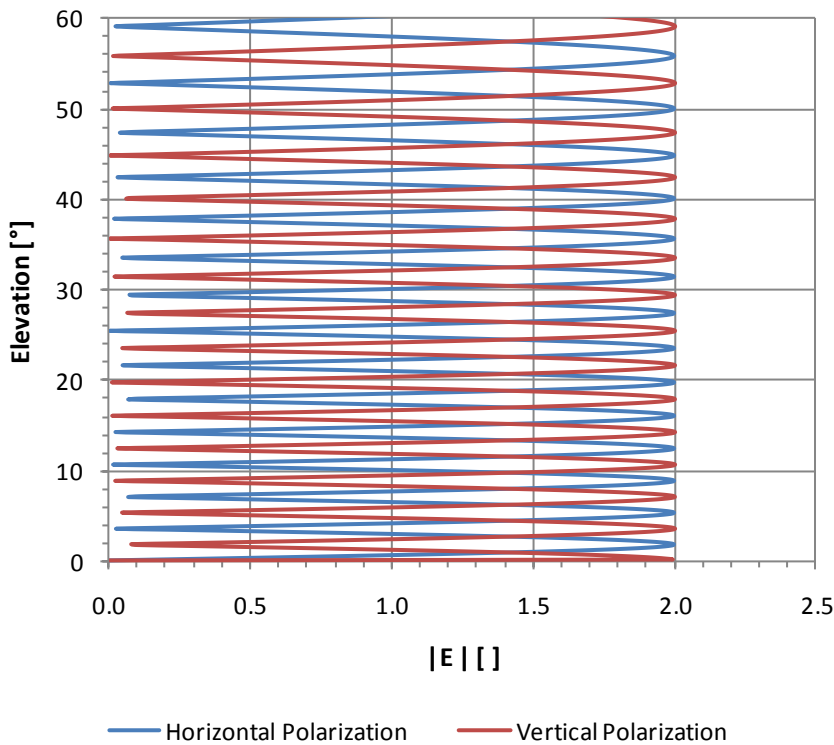
Fig. 4 : Magnitude of the electric field on flat, perfect ground

We see in Fig. 4 that for both polarizations the magnitude of the electric field **E** is doubled at the elevations angles where constructive interference of direct and reflected waves occurs, while nulls occur at elevation angles where the interference is destructive. Things differ in the way maxima in vertical polarization occur at the same elevation angles as the nulls in horizontal polarization. The Ground Gain (in terms of power) is proportional to the square of the modulus of the electric field **E**, so the Ground Gain (GG) in dB will be $GG = 10 * \log(|E|^2)$, as depicted on Fig. 5 below :
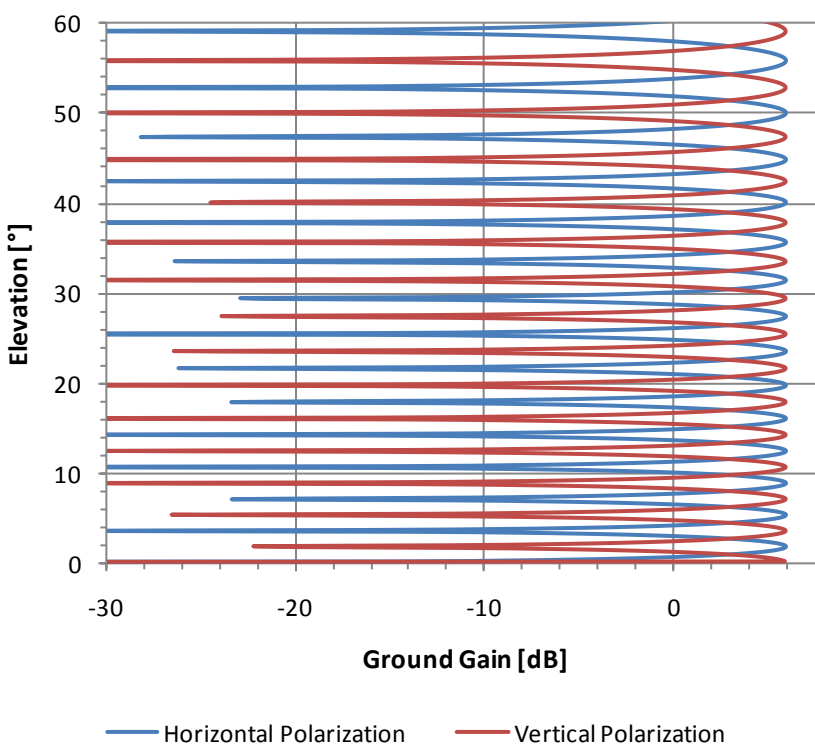
Fig. 5 : Magnitude of the Ground Gain on flat, perfect ground

As shown (Fig. 5), the maximum Ground Gain amounts to 6 dB for each polarization and for a perfect ground plane, the nulls will be theoretically infinite in depth.

So far we have been considering only an isotropic radiator. To see the effect of a perfectly conducting ground plane on a beam antenna, we have to multiply the values shown on the Ground Gain graph above (Fig. 5) with the far field pattern of this antenna (in practice, we use dB scales, so we add or subtract).

Let's consider here a 12-element DK7ZB antenna (16.4 dBi free space gain) in horizontal polarization. The elevation radiation pattern (H-plane or vertical plane) can easily be exported out of an antenna modelling tool (I'm used to MM-ANA [2] or 4NEC2 [3]) and further processed in a MS Excel (or equivalent) spreadsheet. Plotting that processed data gives Fig. 6 :
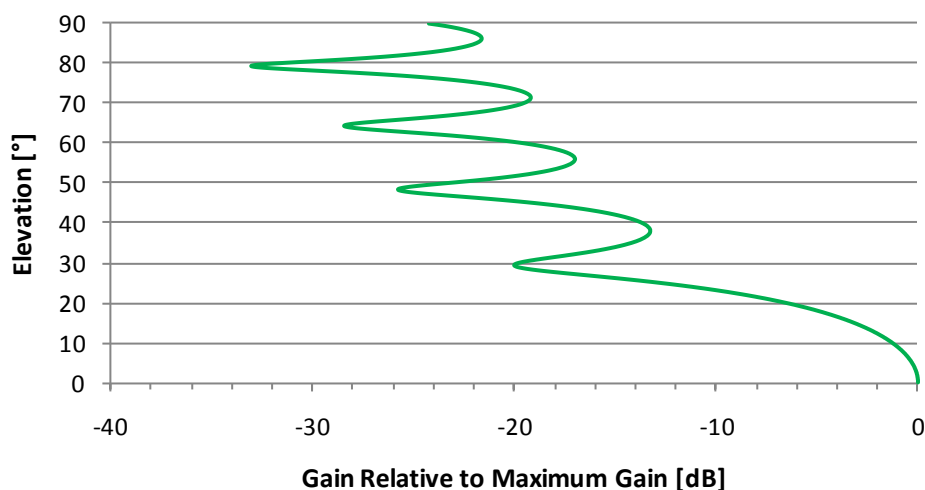
Fig. 6 : Elevation pattern of a 12-element DK7ZB Yagi in free space

If we assume the (free space) antenna radiation pattern is the same in the elevation plane for both horizontal and vertical polarizations, we get Fig. 7 for the Ground Gain in dB :
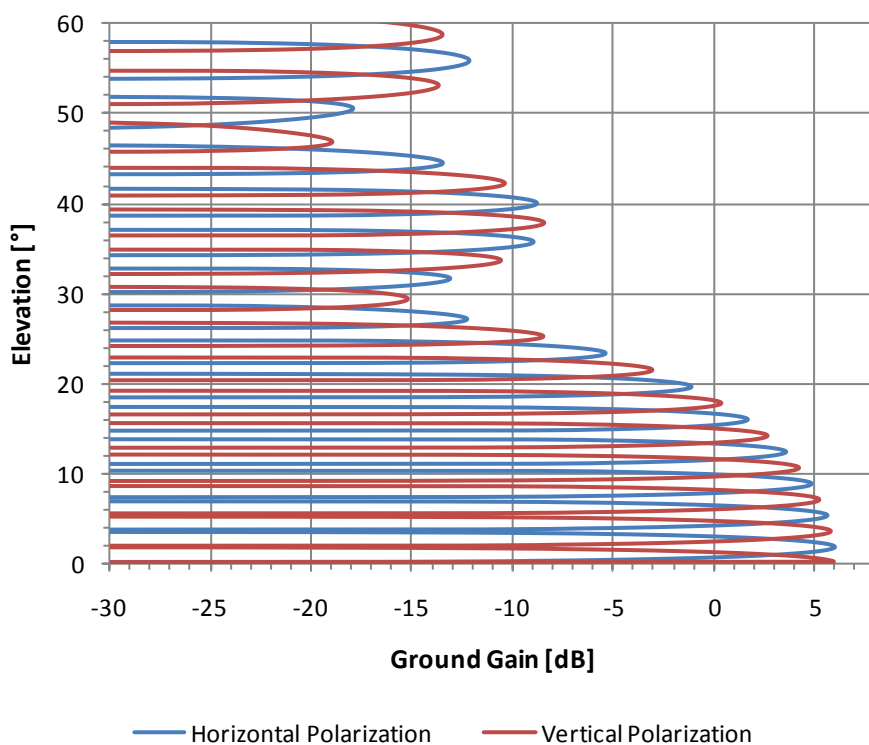
Fig. 7 : Elevation patterns of a 12-element DK7ZB Yagi over a perfect ground plane

When modelling the same antenna in MM-ANA or 4NEC2 at same height over a perfect conductor, we get exactly the same results regarding the elevation of the maxima and the magnitude of the lobes.

With this cross check, we can validate the method explained up to now and conclude that, at some elevation angles, the extra 6 dB of Ground Gain can make a single antenna over ground have the same gain as a stack of four in free space. This said, the gain in the azimuth plane (horizontal) remains the same as that of a single antenna ; which is also a characteristic of a vertical stack.

However, a real stack of four antennas will have 6 dB of gain of its own plus further Ground Gain enhancement.

4. Real Ground Plane

4.1. Reflective Properties of a Real Ground

In the real world, the ground is never a perfect plane conductor ! Taking an analogy with the optical world and considering water, when you are in the water up to the knees at the beach and when you have a look downwards, you can see your feet through the water surface. When you elevate the eyes to the horizon, you don't see any more what is going on inside the water but you see the sun reflecting on the water surface. However, water is not a mirror but it reflects the light nevertheless.
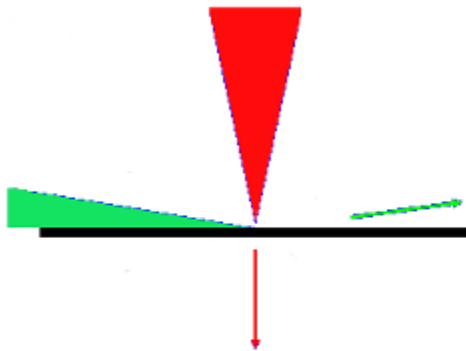
Fig. 8 : Steep angles transmit the most, while shallow (grazing) angles reflect

As shown on Fig. 8, steep angles transmit the most, while shallow grazing angles reflect the most. This is also what happens in the ionosphere for HF propagation : vertical (90°) incidence sends back to earth waves at relatively low frequencies while higher frequencies get through the layer. Changing the incidence angle (from 90° to a lower value), these same higher frequencies will start to be more and more reflected back to earth (actually successively refracted) as the incidence angle is decreased. Thus we see that the ground, although not a perfect conductor, can reflect waves under certain conditions. This is because "reflection" and "transmission" are not two separate phenomena ; in reality, they are only special cases of one broader phenomenon which also includes scattering, diffraction and attenuation (absorption).

All these phenomena occur simultaneously, what varies from one case to another is how much of each phenomenon is present and observable. To achieve "good" or so-called "specular" reflections, the needed conditions are :

- The change or discontinuity between the propagation medium and the reflective surface should be as sharp as possible. The sharper the discontinuity, the better the reflection. The greater the change in dielectric constant, the better the reflection.
- Irregularities on the reflective surface must be small as compared with the wavelength ; the smaller the irregularity, the better the reflection. Alternatively, the longer the wavelength (the lower the frequency), the better the reflection.
- The lower the angle of the incident ray to the discontinuity surface, the better the reflection. At very shallow grazing angles, reflections are best of all.

If these conditions are not fully met, the reflection may be lossy. Losses can include absorption (transmission into the ground) and also a diffuse or scatterer reflection caused by surface roughness as shown in Fig. 9 [4].
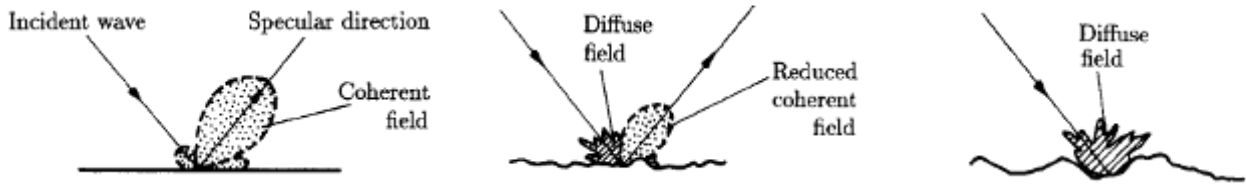
Fig. 9 : Losses due to diffuse or scattered reflection

The reflective properties of a real ground (a perfectly smooth plane but not a perfect conductor) are governed by its dielectric constants :

- The relative permittivity ε_r [ ]   ([ ] = a dimensionless ratio)
- The conductivity σ [S/m] (1 S/m = 1/Ω.m)

Both of them are embedded in the complex permittivity ε' :

$$\varepsilon' = \frac{\varepsilon}{\varepsilon_0} - j * \left(\frac{\sigma}{2 * \pi * f * \varepsilon_0}\right) = \varepsilon_r - j * \left(\frac{\sigma}{2 * \pi * f * \varepsilon_0}\right)$$

ε : absolute permittivity [F/m]
ε_0 : permittivity of the vacuum, 8.854*10^{-12} [F/m]
f : frequency [Hz]

Here are the dielectric constants of some common soil types at low frequencies [5] :

	Conductivity σ [S/m]	Permittivity ε_r [ ]
Poor	0.0010	4.5
Moderate	0.0030	4.0
Average	0.0075	12.5
Good	0.0150	20.0
Dry, Sandy, Flat (Coastal Land)	0.0020	10.0
Pastoral Hills, Rich Soil	0.0065	17.0
Pastoral Medium Hills and Forestation	0.0050	13.0
Fertile Land	0.0020	10.0
Rich Agricultural Land (Low Hills)	0.0100	15.0
Rocky Land, Steep Hills	0.0020	12.5
Marshy Land, Densely Wooded	0.0075	12.0
Mountainous/Hilly (to about 1000 m)	0.0080	12.0
Highly Moist Ground	0.0010	5.0
City Industrial Area of Average Attenuation	0.0125	30.0
City Industrial Area	0.0010	5.0
Fresh Water	0.0001	3.0
Sea Water	0.006	81.0
Sea Ice	4.500	81.0
Polar Ice	0.001	4.0

Table 1 : Dielectric constants of common soil types

4.2. Reflection Coefficients

Now, let's assess how a real ground affects the reflection of a wave through the reflection coefficient **ρ**, governed by the following equations [6] :

For vertical polarization :   For horizontal polarization :

$$\boldsymbol{\rho_v} = \frac{\varepsilon' * \sin(\alpha) - \sqrt{\varepsilon' - \cos^2(\alpha)}}{\varepsilon' * \sin(\alpha) + \sqrt{\varepsilon' - \cos^2(\alpha)}} \qquad \boldsymbol{\rho_h} = \frac{\sin(\alpha) - \sqrt{\varepsilon' - \cos^2(\alpha)}}{\sin(\alpha) + \sqrt{\varepsilon' - \cos^2(\alpha)}}$$

We see that these coefficients are complex numbers (through the complex permittivity) ; they are also frequency dependant.

If we convert the term under the square root into its polar form (using conversion equations given in section 3.2.) and apply DeMoivre's theorem which states :

$$\left(|z| * e^{jx}\right)^n = |z|^n * e^{jnx}$$

Where, for a square root, n=1/2 and if we then convert back to the Cartesian form, we will find an equation of the form :

$$\boldsymbol{\rho_{v,h}} = \frac{(a + j * b) + (c + j * d)}{(p + j * q) + (r + j * s)} = \frac{(a + c) + j * (b + d)}{(p + r) + j * (q + s)}$$

In the case of the horizontal polarization, b and q are equal to 0.

Next we apply the identity :

$$\frac{v + j * w}{x + j * y} = \left(\frac{v * x + w * y}{x^2 + y^2}\right) + j * \left(\frac{w * x - v * y}{x^2 + y^2}\right)$$

And then finally back to the polar form, we then see the reflection coefficients expressed as :

For vertical polarization :   For horizontal polarization :

$$\boldsymbol{\rho_v} = |\rho_v| * e^{j\theta_v} = |\rho_v| * \cos(\theta_v) + j * |\rho_v| * \sin(\theta_v) \qquad \boldsymbol{\rho_h} = |\rho_h| * e^{j\theta_h} = |\rho_h| * \cos(\theta_h) + j * |\rho_h| * \sin(\theta_h)$$

As an example, let's consider sea water with its dielectric constants of :

- ε_r = 81 [ ]
- σ = 4.5 [S/m]

If we now perform the above calculation of $|\rho_{v,h}|$ and $\theta_{v,h}$ as a function of α from 0° to 90° (using MS Excel or equivalent) and plot the results, we have Fig. 10 and Fig. 11 :
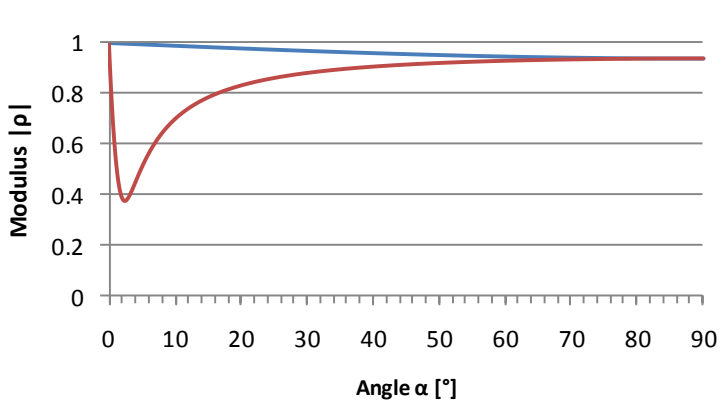
Fig. 10 : Sea water reflection coeff. modulus

Fig. 11 : Sea water reflection coeff. phase

For sea water, a good natural conductor with a high dielectric constant, we see that the modulus of reflection for horizontal polarization is close to the ideal value of 1, especially at low angles, while the phase stays very close to the ideal value of 180°. But vertical polarization is very different ! Here we see a sharp dip in the modulus, accompagnied by a sharp fall in the phase angle from 180° towards the idealized value of 0°. The angle at which the modulus of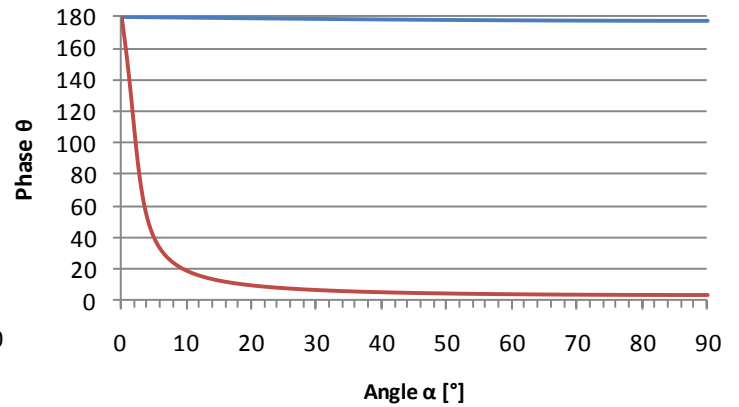 the reflection coefficient for vertical polarization is a minimum is called the "pseudo-Brewster angle". It is also the angle at which a phase shift (from 180° towards 0°) occurs.

If we go back for a moment to the original case of the perfectly reflective plane (section 3.2.), the reflection coefficient was also applicable but we didn't highlight it at that time ; we also spoke about a phase shift but we didn't mention any magnitude change due to the reflection, because there isn't one in that idealized case. If we had plotted the reflection coefficients for vertical and horizontal polarizations in the same formats as Fig. 10 and Fig. 11, we would have had Fig. 12 and Fig. 13 :
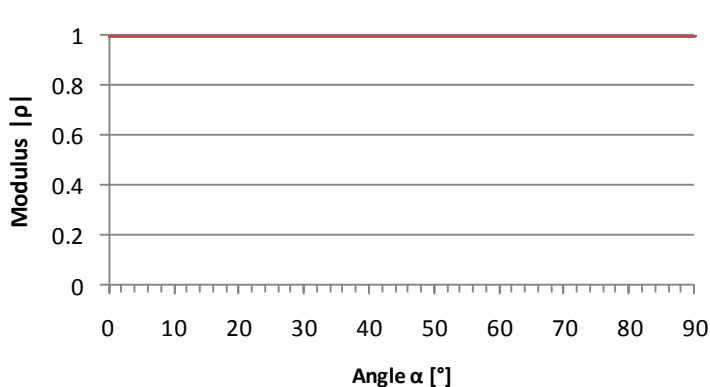
Fig. 12 : Idealized reflection coeff. modulus
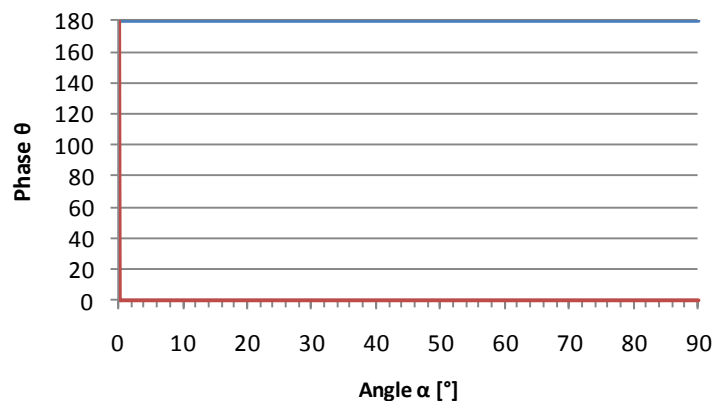
Fig. 13 : Idealized reflection coeff. phase

Fig. 12 and Fig. 13 show a perfect (non-lossy) reflection with $|\rho_v| = |\rho_h| = 1$ and ground reflection induced phase shifts of 180° (θ_h) and 0° (θ_v) for horizontal and vertical polarizations respectively.

Comparing Fig. 10 with Fig. 12 and Fig. 11 with Fig. 13, we see that by far the greatest differences are for vertical polarization.

4.3. Magnitude and Geometry of the Antenna Lobes

The mathematical formulas for a real ground are similar to the ones shown in section 3.2. for perfect ground, but they need to be a bit updated as follows.

The total phase shift of the reflected wave is : $\Delta = \delta + \theta_{v,h}$

The electric field of the direct wave remains unchanged, so : $\mathbf{E_{direct}} = 1 * e^{j0} = 1 + j * 0$

But the expression of the electric field of the reflected wave becomes :

$$\mathbf{E_{reflected}} = \left|\rho_{h,v}\right| * e^{j\Delta} = \left|\rho_{h,v}\right| * \cos(\Delta) + j * \left|\rho_{h,v}\right| * \sin(\Delta)$$

And the total electric field is now :

$$\mathbf{E} = \mathbf{E_{direct}} + \mathbf{E_{reflected}} = \left(1 + \left|\rho_{h,v}\right| * \cos(\Delta)\right) + j * \left|\rho_{h,v}\right| * \sin(\Delta)$$

If we calculate the modulus of the electric field, we come up with :

$$|E| = \sqrt{1 + 2 * \left|\rho_{h,v}\right| * \cos(\Delta) + \left|\rho_{h,v}\right|^2}$$

Plotting the Ground Gain $GG = 10 * \log(|E|^2)$ for a sea water reflective surface, taking into account the antenna pattern in the same way as above gives Fig. 14 :
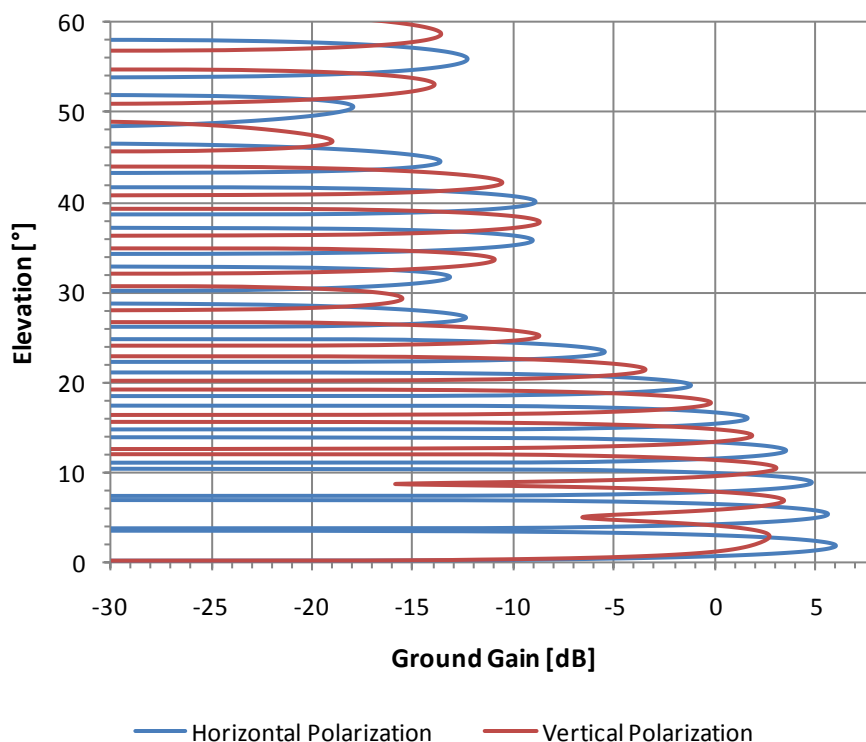
Fig. 14 : Reflections over sea water

Compared to a perfectly conductive plane, the elevation angles for the horizontal polarization over sea water are little changed and the magnitude of the lobes is only very slightly lowered. The vertical polarization is much more affected, both regarding the elevation angles and the magnitude of the lobes. But if we now change to poor ground, what happens is very different, as shown in Fig.15 :
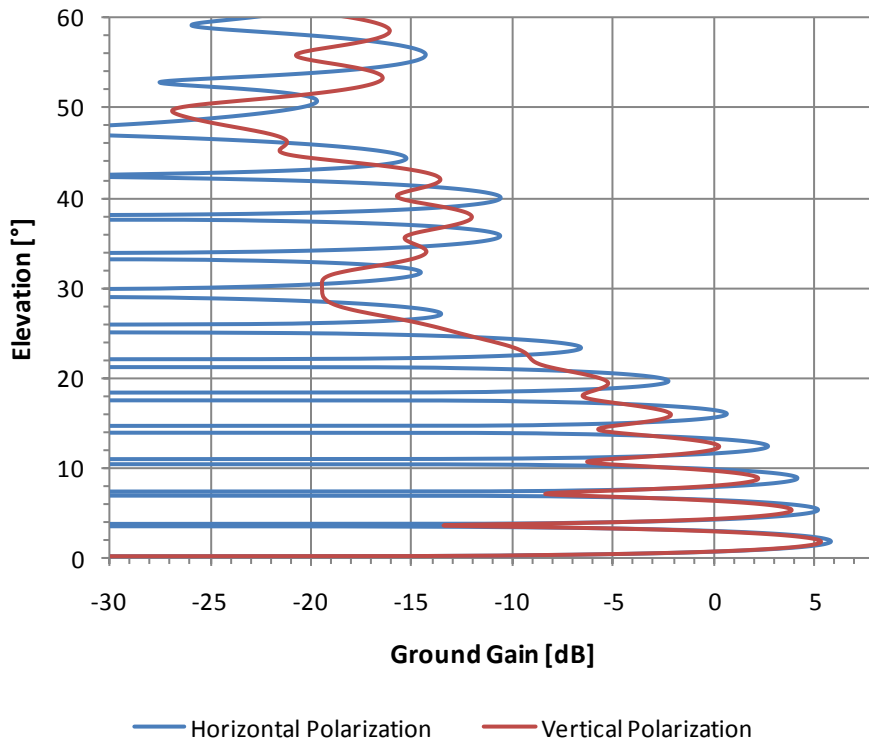
Fig. 15 : Reflections over poor ground

Relative to a perfectly reflective plane, we see that that the magnitude of the upper lobes is lower, both for horizontal and vertical polarizations.

All the calculations and graphs above have been made thanks to a MS Excel (2007) spreadsheet (Ground Gain Geometry and Magnitude Calculator File.xlsx) which is available for download on my website [7].

4.4. Lobe Building Distance from the Antenna

An important point that was not shown in Fig. 1 and Fig. 2 is that reflections do not take place at a single point. A significant surface area on the ground is necessary to construct the reflected wave front, and this is governed by the first Fresnel zone geometry (Fig. 16).

Fig 16 : Fresnel zones on the ground are required to construct the reflected wave front

This has been well described in the article of Palle, OZ1RH [1a]. I have been lucky enough to find the book "Proceedings of the IRE – Scatter Propagation Issue" [1b] which Palle refers to in his article. The relevant extracts are available for download on my website [7]. So, I don't reproduce the formulas here.
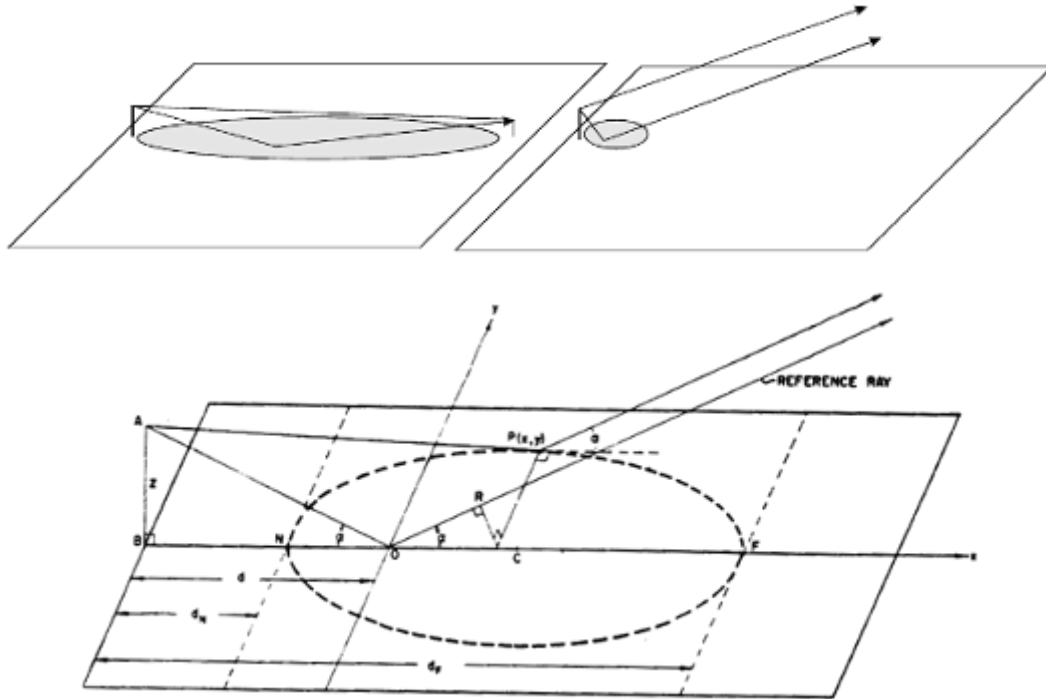
Still using the same example of the 12-element DK7ZB antenna at 17m agl, we can now calculate the Fresnel ellipsoid dimensions :

Distance from antenna where the **maximum** of the **first lobe** builds (d) : 574m
Closest distance from antenna as from which first ground lobe builds (d_N) : 98m
Furthest distance from antenna up to which first ground lobe builds (d_F) : 3348m
Width of the Fresnel ellipsoid (w) : 98m

Those figures may be amazing ; the reflection surface is much larger than most people imagine.

As a cross-check, let us compare d (distance from antenna), calculated with the first Fresnel zone geometry versus the one calculated with the geometry considered in the preceding sections of the present article. The results are quite close (Fig. 17) so the calculations about the enormous size of the first Fresnel zone really are true !
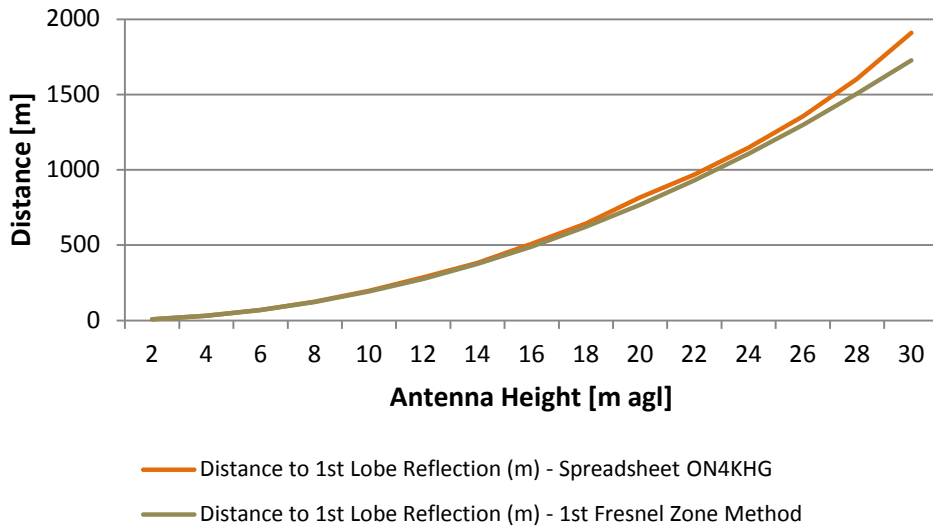
Fig. 17 : Distance between antenna and reflection spot of 1ˢᵗ lobe maximum vs antenna height

4.5. Comparison between Two Antennas

Two more interesting facts deserve a few words. The first point lies in comparing a "high gain" antenna (narrow radiation pattern) with a lower gain one (broader radiation pattern). For this purpose, a 12-element DK7ZB - 16,4 dBi and a 8-element G0KSC - 14 dBi have been modelled (4NEC2).
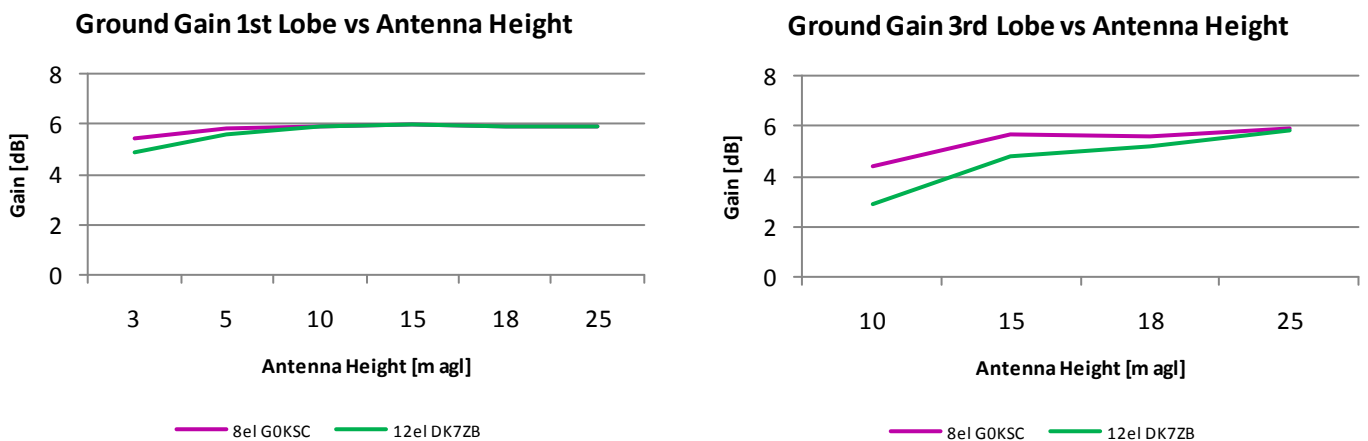
Fig. 18 : Development of Ground Gain for two different antennas

Fig. 18 shows "how fast" the maximum Ground Gain is developed according to the antenna type and height. On the first elevation lobe, both antennas exhibit the maximum gain as from 10m high. At lower heights, the 8-element exhibits a slightly higher Ground Gain.

On the third elevation lobe, a height of 25m must be reached before both antennas achieve their maximum Ground Gain. Below this height, the 8-element produces a significantly higher Ground Gain than the 12-element.

The second point is about comparing the difference in total gain (i.e. including the Ground Gain) versus elevation, for the same antennas as above, located respectively at 10, 15 and 25m agl. See Fig. 19.

Ground Gain vs Elevation (Antenna @ 10m agl)

Ground Gain vs Elevation (Antenna @ 15m agl)

— Delta Total Gain (incl. GG) DK7ZB vs G0KSC Antennas
— Absolute GG G0KSC Antenna
— Absolute GG DK7ZB Antenna
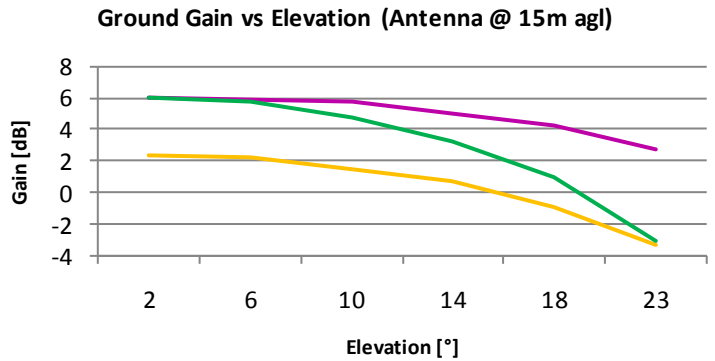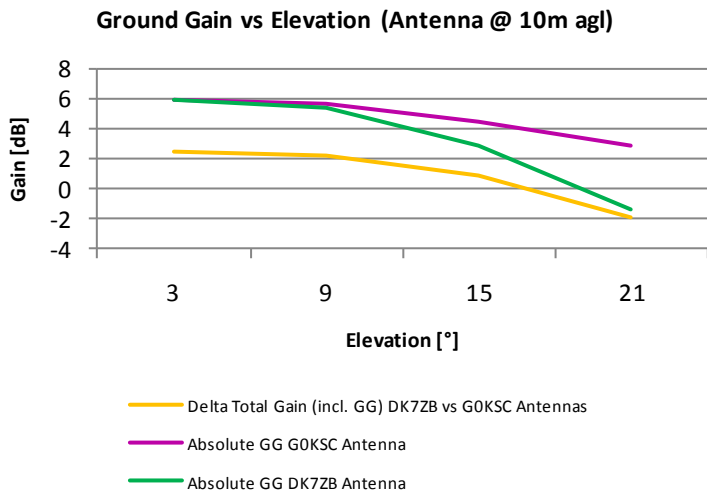
Fig. 19 : Ground Gain for two different antennas, at three different heights

Ground Gain vs Elevation (Antenna @ 25m agl)

The curve in green indicates the Ground Gain produced by the 12-element ; the one in purple, the Ground Gain of the 8-element and the curve in yellow is the difference ("delta") between both antennas, taking into account each antenna's own free space gain plus Ground Gain of each antenna. We notice that despite the 2.4 dB (16.4-14) of extra free space gain in favour of the 12-element, the overall difference reaches zero at a certain elevation angle, and above this angle the predicted total gain of the smaller 8-element is superior to the 12-element. These elevation angles are 16.9° when the antennas are 10m agl, 15.7° at 15m and 18° at 25m. This "crossover" in performance happens because the 12-element has a narrower vertical (and horizontal) radiation pattern so it is less able to take advantage of the Ground Gain available at higher elevation angles. It can be concluded that in order to take advantage of the Ground Gain available at all elevation angles, the antenna should preferably not have too much gain of its own.
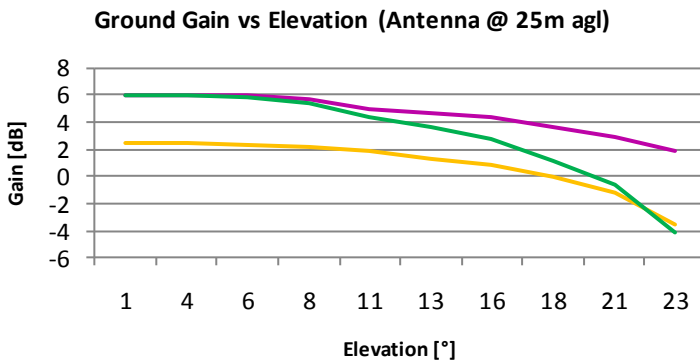
4.6. Conclusion

After having run several simulations by changing the different parameters, we can draw the following general conclusions.

	Vertical Polarization	*Horizontal Polarization*
Antenna height (1/3)	The higher the antenna, the lower the elevation angle of the first Ground Gain lobe.	The same.
Antenna height (2/3)	The higher the antenna, the more and the narrower the lobes and the nulls.	The same.
Antenna height (3/3)	The higher the antenna, the further from the antenna and the wider the surface on the ground needed for the lobes to build.	Same behavior but lobe building occurs even further away from the antenna than for vertical polarization. For highly conductive real grounds, it is twice the distance for a perfectly conductive ground.
Ground properties	Elevation angles at which Ground Gain is achieved are very dependant on the ground properties.	Ground Gain lobes always occur at the same elevation angles, no matter the ground properties.
Magnitude of the lobes (1/2)	The more Ground Gain at the elevation maxima, the deeper the nulls.	The same.
Magnitude of the lobes (2/2)	The magnitude is very dependant of the ground properties (and the pseudo-Brewster angle). For instance, sea water (highly conductive) exhibits a lower magnitude on the first lobe than in the subsequent more highly elevated lobes (but still less compared to horizontal polarization). However, for a poor ground, the difference of magnitude of the first lobe is very tight compared to the horizontal polarization (5.5 dB for vertical compared with 6 dB for horizontal), while this same difference increases for the more elevated lobes (less and less gain for vertical versus horizontal polarizations).	The magnitude of the first lobe (grazing angle) can easily reach 6 dB for any ground type (highly or poorly conductive). The magnitude of the more highly elevated lobes suffers more of the reflective properties of the ground (and the free space antenna radiation pattern too, but this is implicit), the incidence angles being less and less grazing.
Sloping ground	Same behavior as above but the Ground Gain elevation angles are lower than for a flat ground (heading more towards the horizon than the sky) and the distance where the lobes build is much closer to the antenna than for a flat ground.	
Near field	Some highly elevated lobes build very close to the antenna, where the near field still prevails and hence where the radiation pattern of the antenna is not built yet. The validity of these lobes is very questionable.	
Radiation pattern	We have assumed so far that (except for the effect of the reflection coefficient on the magnitude of the reflected wave), the direct and reflected waves have the same magnitude far away from the antenna. This is true for the low elevation angle lobes, for which the reflected wave is originating from close to the maximum of the (free space) antenna radiation pattern. The high elevation lobes are made up of reflections close to the antenna and then the wave front originating from the antenna is already well attenuated by the radiation pattern of the antenna. Hence, the highly elevated lobes have actually a lower magnitude than depicted on the graphs. This is even more true for the high gain antennas (narrow radiation pattern) and/or for a sloping ground (reflections building closer from the antenna than for a flat ground).	
Frequency	This page focuses on 144 MHz but it is worthwhile to mention that given the height of a 432 MHz antenna compared to the wavelength, the lobe pattern will be made up of many narrow successive maxima and nulls. Also, because the ground irregularities must be small compared to the wavelength in order to give good specular reflections, the likelihood for useful Ground Gain on 432 MHz at most locations is not very high. In other words, the ground appears less and less "flat" (or assumed to be so) as the frequency increases. Finally, vertical polarization is more frequency dependant than horizontal polarization.	

Table 2 : General conclusions about the theoretical aspects

5. Ground Gain Measurement using the Sun Noise

5.1. Introduction

In the preceding sections, we have been dealing so far with theoretical concepts about the Ground Gain geometry and magnitude, over flat horizontal or tilted grounds of given reflective quality.

However, some short cuts have been taken as :

- Perfect flatness is not often applicable in reality. Terrain irregularities and clutter (building and vegetation) introduce scattering/diffraction and attenuation
- According to the wavelength, the radio waves are more or less penetrating into the ground when hitting it ; while here, we have only considered a sharp boundary between the air and the ground
- The ground conductivity and permittivity have been considered constant and uniform over the whole reflective surface. This is not the case in reality
- We have considered a "two rays" model, i.e. a direct wave issued by the antenna and its reflected wave (resulting in 6 dB Ground Gain enhancement at best). In reality, there can be environments (sloping ground towards the sea, mountain valleys,...) where there can be more than two paths leading to constructive interference (over very narrow lobes and hence very limited time span in case of signals being received from a moving object like the moon). In these specific cases, the Ground Gain enhancement can amount to more than 6 dB (12 dB in case of four paths)

It is almost impossible to expand the theory to take all of these factors accurately into account. Instead, the goal of the present and coming sections is to assess one's own actual Ground Gain geometry and magnitude through practical measurements, using the noise generated by the sun.

5.2. Receiving Station Data

A typical 144 MHz station is used as a case study to support the calculation and the development of the measurement procedure ; it is actually my own station.

Fig. 20 and Table 3 show respectively the receiving station bloc diagram and the overall system spreadsheet.

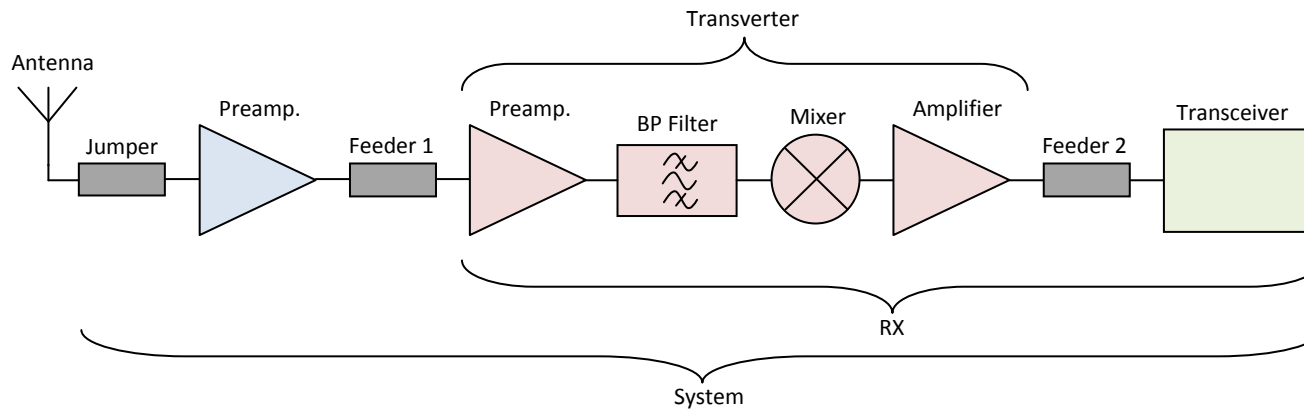The antenna is a single 12-element (4 λ, 16.4 dBi) DK7ZB at 17m agl.

Fig. 20 : Receiving station bloc diagram

	Antenna	*Jumper*	*Preamp. (External)*	*Feeder 1*	*Preamp. (Transverter)*	*Band-Pass Filter*	*Mixer*	*(Post-mixer) Amplifier*	*Feeder 2*	*Transceiver*
Gain G [dB(i)]	G_{ant} : 16.30	G_1 : -0.10	G_2 : -0.10	G_3 : -0.80	G_4 : 22.00	G_5 : -2.00	G_6 : -7.00	G_7 : 9.00	G_8 : -4.00	
Gain g [ ]	42.66	g_1 : 0.98	g_2 : 0.98	g_3 : 0.83	g_4 : 158.49	g_5 : 0.63	g_6 : 0.20	g_7 : 7.94	g_8 : 0.40	
Noise Figure NF [dB]		NF_1 : 0.10	NF_2 : 0.10	NF_3 : 0.80	NF_4 : 0.40	NF_5 : 2.00	NF_6 : 7.00	NF_7 : 2.50	NF_8 : 4.00	NF_9 : 6.00
Noise Factor f [ ]		f_1 : 1.02	f_2 : 1.02	f_3 : 1.20	f_4 : 1.10	f_5 : 1.58	f_6 : 5.01	f_7 : 1.78	f_8 : 2.51	f_9 : 3.98
Noise Temp. T [K]	See sect. 5.4.	T_1 : 6.75	T_2 : 6.75	T_3 : 58.66	T_4 : 27.98	T_5 : 169.62	T_6 : 1163.4	T_7 : 225.7	T_8 : 438.45	T_9 : 864.51
Purpose of the stage		The coaxial section (that allows antenna rotation) between the antenna radiating element and preamp. or junction with feeder	Preamp. set in **by-pass mode** to ease calculations. So, the **insertion loss** is considered here	The coaxial section between the preamp. or junction with jumper and the Transverter (or Transceiver) input	First RX stage of the Transverter (or Transceiver)				The coaxial section between the Transverter output and the IF Transceiver	

Table 3 : Overall system spreadsheet

The figures in red are the ones that must be known and which serve as input, out of which the figures in black are calculated. Since the attenuation (A) of a **lossy stage** (filter, attenuator, cable,...) is known, its Noise Figure (NF) is also known, as it amounts to the same figure.

$$f = \frac{1}{g} = a \qquad\qquad NF = 10 * \log(f) = -G = A$$

<div align="center">

f : Noise Factor [ ]   NF : Noise Figure [dB]

g : Gain [ ]   f : Noise Factor [ ]

a : Attenuation [ ]   G : Gain [dB]

A : Attenuation [dB]

</div>

To convert between gain in dB (first line in Table 3) and gain as a ratio (second line), we have to calculate : $g = 10^{\left(\frac{G}{10}\right)}$

In a similar way (for third and fourth lines in Table 3), we have : $f = 10^{\left(\frac{NF}{10}\right)}$

From a general point of view (when no square-law is involved), to convert a value X in dB into a one, x, in ratio : $x = 10^{\left(\frac{X}{10}\right)}$

And to convert ratios into dB's : $X = 10 * \log(x)$

To calculate the figures of the fifth line in the table, we use : $T = (f - 1) * T_0$

Where T is the noise temperature in Kelvin [K] and T_0 is the reference temperature ("room" temperature) of 290 K (17°C or 62°F).

5.3. Measurement Setup

The radio hardware used is as described in section 5.2. The loudspeaker or data output of the transceiver is connected to the input of the soundcard of a computer, running a software able to record the audio noise power. I have been successfully using either "Spectrum Lab" by DL4YHF [8] or "WSJT 9" in Measure mode, by Joe K1JT [9]. The configuration files and screenshots are available for download on my website [7]. These tools allow one to export measurement data in text file format that will be further processed in MS Excel (or equivalent). "Spectrum Lab" also allows the user to periodically take screenshot captures of the audio spectrum (useful to assess the presence of disturbing signals during the measurement). The following precautions must be observed to ensure the most accurate measurements possible :

- Transceiver AGC (Automatic Gain Control) set to OFF
- Whole receiving chain (RX and soundcard) assumed to be linear (and confirmed by repeating the same measurement at higher and lower signal levels)
- Transceiver Noise Blanker (NB) set to ON. The white noise to be measured is normally not altered by the NB, while the pulse noises (disturbing the measurement) will be suppressed (but again this assumption must be verified)
- A clear frequency, not subject to disturbances (QRM)
- The whole station and computer powered ON at least 12 hours before performing the measurement, so that the whole setup is stable and at temperature during the measurement
- Good weather with no wind or rain to avoid static noise

5.4. Preliminary Calculations

5.4.1. Reference noise level definition (calibration)

This step is easily achieved by connecting a 50Ω load at the input of the Transverter (see Fig. 21).
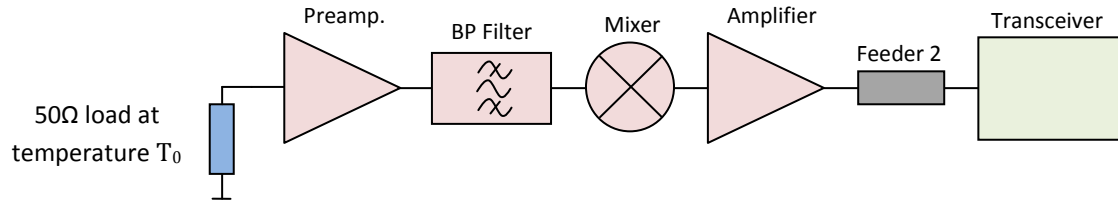
Fig. 21 : Setup for calibration

This setup will produce a certain measured noise level on the audio analyser. Given that the noise contribution (noise temperature) of a resistor (load) is the same as its physical temperature, the 50Ω load at a known absolute temperature T_0 (assumed here to be 290 K) leads to : $T_{load} = T_0 = 290$ K

And we can write : $T_{reference} = T_{load} + T_{RX}$

$T_{reference}$ is the noise temperature of the whole system, including both the load and the RX, that give rise to the "certain" noise level (as named so above) on the audio analyser.

Hence, we have now to calculate the contribution of the RX in $T_{reference}$ using the Friis noise formula :

$$T_{RX} = T_1 + \frac{T_2}{g_1} + \frac{T_3}{g_1 \cdot g_2} + \cdots + \frac{T_n}{g_1 \cdot g_2 \cdots g_{n-1}}$$

By substituting with the corresponding figures of the table in section 5.2., we come up with :

$$T_{RX} = T_4 + \frac{T_5}{g_4} + \frac{T_6}{g_4 \cdot g_5} + \frac{T_7}{g_4 \cdot g_5 \cdot g_6} + \frac{T_8}{g_4 \cdot g_5 \cdot g_6 \cdot g_7} + \frac{T_9}{g_4 \cdot g_5 \cdot g_6 \cdot g_7 \cdot g_8} = 68.5 \text{ K}$$

And $T_{reference} = 290 + 68.5 = 358.5$ K

Knowing that the noise power n is proportional to the noise temperature T, as $n = k * T * B$ (Nyquist Equation)

n : noise power [W]
k : Boltzmann constant, 1.381*10^{-23} [J/K]
B : bandwidth [Hz]

We can state : $n_{reference} = k * (T_{load} + T_{RX}) * B$ as the noise power generated (in W/Hz) by the RX connected to the 50Ω load. $N_{reference}$ is the same but expressed in dBW/Hz :

$$N_{reference} = 10 * \log(n_{reference})$$

The figure displayed by the audio analyser in the course of a measurement is simply the "image" (a figure directly related to) of $N_{reference}$.

5.4.2. Background Noise Assessment

Here, we disconnect the 50Ω load from the RX input and we connect the antenna through the antenna line made up of the jumper, the preamp. (in by-pass mode) and the feeder 1 (see Fig. 22).

The antenna pointing towards the horizon (no elevation) will pick-up :

- Its own antenna noise (resistive losses and thermal noise)
- The ground noise (noise generated by the earth)
- The sky noise (galactic noise)
- The man-made noise (industrial, urban,... noises due to human activities)

All these noises will come up at the antenna radiating element terminals through its main, side and rear lobes and some of the noise will arrive by reflection off the ground. We gather all these noise contributions under the so-called "Antenna Noise Temperature", T_{ant}, that we rename here $T_{ant\ bgd}$ ("bgd" standing for "background"). Hopefully, the measured noise level on the audio analyser should at least rise a bit by performing this operation (connecting the antenna in place of the 50Ω load) ; otherwise, you have to check your RX setup capabilities. Also note that even a small deviation of antenna impedance from 50Ω can dramatically change the gain of some preamplifiers [16] and this variation could affect the entire measurement through its effect on the spreadsheet (Table 3).

We can gather all the losses related to the antenna line (the jumper, the preamp. in by-pass mode and the feeder 1) into a single stage named "Ant. line losses", of which the total gain is :

$$G_{Ant.\ line\ losses} = G_1 + G_2 + G_3 = -1\ dB$$

Or $A_{Ant.\ line\ losses} = -G_1 - G_2 - G_3 = 1\ dB$

Or also $a_{Ant.\ line\ losses} = \frac{1}{g_1 \cdot g_2 \cdot g_3} = 1.25$

The setup is depicted below in Fig. 22 :
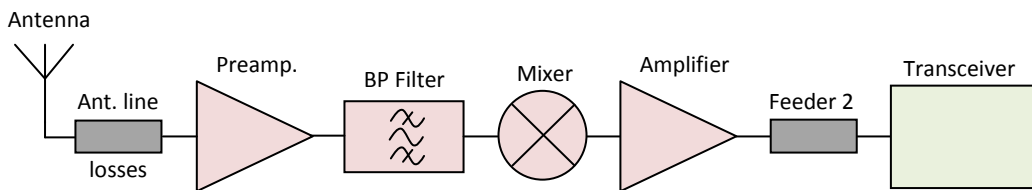
Fig. 22 : Setup for background and sun noise measurements

Since the antenna can be seen as a 50Ω load at a noise temperature $T_{ant\ bgd}$ and since T_{RX} has been calculated in section 5.4.1., we come up with Fig. 23 :

Fig. 23 : Including the antenna's background noise temperature

As the reference noise level has been set up at the RX input (section 5.4.1.), we have here to introduce a correction factor that reflects how the 50Ω load at $T_{ant\,bgd}$ in front of the "Ant. line losses" stage looks 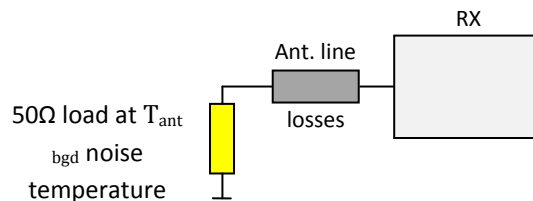like at the RX input (not in front but after the antenna line stage). Obviously, the antenna noise will be attenuated by the amount of the loss of the "Ant. line losses" stage. Moreover, the "Ant. line losses" stage being a lossy stage mainly made up of coaxial cable, it generates a thermal noise, so that :

$$T_{ant\,bgd\,corrected} = \frac{T_{ant\,bgd}}{a_{Ant.\,line\,losses}} + [(f_{Ant.\,line\,losses} - 1) * T]$$

The first term represents the noise temperature decrease due to the loss and the second term represents the thermal noise generation. We have seen in section 5.2. that the noise factor f of a lossy device equals its attenuation a. If T is the physical temperature of the cable, here assumed to be 290 K (or T_0), we can then write :

$$T_{ant\,bgd\,corrected} = \frac{T_{ant\,bgd}}{a_{Ant.\,line\,losses}} + [(a_{Ant.\,line\,losses} - 1) * T_0] = \frac{T_{ant\,bgd}}{1.25} + [(1.25 - 1) * 290]$$

$$T_{ant\,bgd\,corrected} = \frac{T_{ant\,bgd}}{1.25} + 72.5$$

So now we have Fig. 24 :

50Ω load at $T_{ant\,bgd}$ corrected noise temperature
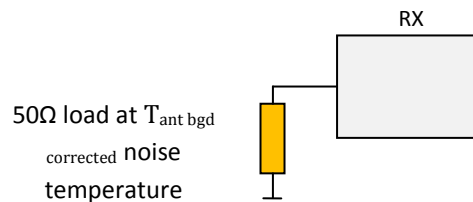
Fig. 24 : Corrected antenna noise temperature

Let's take an example : after connecting the RX input to the antenna line in place of the 50Ω load of section 5.4.1., we measure a 2 dB rise in the noise on the audio analyser (NR_{bgd} in dB). We can now calculate the $T_{ant\,bgd\,corrected}$ and $T_{ant\,bgd}$ that give rise to this measured noise increase.

As in section 5.4.1., we pose : $n_{bgd} = k * (T_{ant\,bgd\,corrected} + T_{RX}) * B$ as the noise power generated (in W/Hz) by the RX connected to the antenna line. N_{bgd} is the same in dBW/Hz.

We have :

$$NR_{bgd} = 2\,dB = N_{bgd} - N_{reference} = 10 * \log\left(\frac{n_{bgd}}{n_{reference}}\right) = 10 * \log\left(\frac{T_{ant\,bgd\,corrected} + T_{RX}}{T_{load} + T_{RX}}\right)$$

Or :

$$nr_{bgd} = 10^{\left(\frac{2}{10}\right)} = 1.585 = \left(\frac{n_{bgd}}{n_{reference}}\right) = \left(\frac{T_{ant\,bgd\,corrected} + T_{RX}}{T_{load} + T_{RX}}\right)$$

Hence :

$$T_{ant\,bgd\,corrected} = \left(nr_{bgd} * T_{reference}\right) - T_{RX} = (1.585 * 358.5) - 68.5 = 499.7\,K$$

And :

$$T_{ant\,bgd} = \left(T_{ant\,bgd\,corrected} - 72.5\right) * 1.25 = (499,7 - 72,5) * 1,25 = 534\,K$$

So, replacing a 50Ω load at a physical temperature of 290 K connected to the RX input by an antenna line ending with an antenna at a noise temperature of 534 K will produce the measured rise of 2 dB in the noise on the audio analyser.

For reasons to be explained in the next section, this background noise measurement has to be made either before sun rise (sun below -5° elevation) or after the sun has risen above 30°. The rise in background noise on the audio analyser is measured in steps of 5 degrees azimuth over the same azimuth range that is about to be used for sun noise measurement (roughly between -5° and 30° elevation). Alternatively the entire procedure can be reversed to use the setting sun.

5.4.3. Ground Gain Magnitude Assessment using the Sun Noise

Now that we have calculated the antenna noise temperature without sun influence, we can measure the amount by which the noise power on the audio analyser will rise in presence of the moving noise source which is the sun.

Taking into account the solar activity level, it is possible to calculate this amount quite easily without any (or very little) ground influence.

For example, we might calculate that the sun will produce a noise rise of say 1.5 dB without ground influence, at some elevation. If we then measure that the noise rise is actually 4 dB at the maximum of a ground reflection lobe, we can conclude that the magnitude of the Ground Gain is 4 − 1.5 = 2.5 dB.

The sun emits massive quantities of electromagnetic waves over a very wide spectrum range. Amongst the many observations performed about the sun, the Radio Solar Flux (RSF) is of particular interest here. The purpose is to measure the flux at several frequencies, each representing a specific area to be observed (lower corona, lower, middle and higher chromosphere) [10].

The US Air Force is operating a worldwide Radio Solar Telescope Network (RSTN), including observatory stations in :

- Learmonth, Australia
- San Vito, Italy
- Sagamore Hill, Massachusetts, USA
- Palehua, Hawaii, USA

The Dominion Radio Astrophysical Observatory in Penticton, British Columbia, Canada also operates such a station.

All together, they measure the Radio Solar Flux at the frequencies of 245, 410, 610, 1415, 2695, 2800, 4995, 8800 and 15400 MHz

The daily report can be found on the website of the US Space Weather Prediction Centre [11].

Here is an example (Fig. 25) :

```
# Prepared by the U.S. Dept. of Commerce, NOAA, Space Weather Prediction Center
# Please send comments and suggestions to SWPC.Webmaster@noaa.gov
#  Units: 10^-22 W/m^2/Hz
#  Missing Data:  -1
#
#    Daily local noon solar radio flux values - Updated once an hour
#
  Freq  Learmonth  San Vito  Sag Hill  Penticton  Penticton  Palehua  Penticton
   MHZ   0500 UTC  1200 UTC  1700 UTC   1700 UTC   2000 UTC  2300 UTC  2300 UTC


2011 Jul 12
   245        16        19        20        -1        -1        -1        -1
   410        37        -1        37        -1        -1        -1        -1
   610        54        -1        48        -1        -1        -1        -1
  1415        81        81        85        -1        -1        -1        -1
  2695        94        93        90        -1        -1        -1        -1
  2800        -1        -1        -1        92        92        -1        92
  4995       142       136       134        -1        -1        -1        -1
  8800       255       250       260        -1        -1        -1        -1
 15400       507       554       552        -1        -1        -1        -1
```

Fig. 25 : Example of typical Radio Solar Flux data

The "-1" indicates either a missing data or the sun is not visible at the time/date of the measurement.

The Radio Solar Flux is expressed in "sfu" (solar flux unit) : 1 sfu = 10^{-22} [W/m^2/Hz]. The reference RSF is taken at 2800 MHz (or at a wavelength of 10.7cm). On the table above, we see that on July 12th, 2011, the RSF was 92 sfu at 2800 MHz. It ranges from 50 (quiet sun) to 300 (very high activity) at 2800 MHz and it is closely linked to the SSN (Sun Spot Number). Many web robots provide SSN data, as well as daily RSF at 2800 MHz, also known as "SFI" (Solar Flux Index). What we need here is the RSF at 144 MHz. I have found two ways to extrapolate the 2800 MHz data down to 144 MHz :

- By using the "EME Calculator" software of Doug, VK3UM [12], which extrapolates or interpolates the RSF on the amateur bands above 30 MHz and up to 47 GHz, out of the daily data (measurement at 8 different frequencies) retrieved from the Australian Learmonth solar telescope
- By using a polynomial curve [13] derived from experimental data. Since the RSF is known at 2800 MHz (RSF_{2800}), it can be calculated for the 144, 432 and 1296 MHz bands using :

  - $RSF_{144} = -0.00037689 * (RSF_{2800})^2 + 0.162242 * RSF_{2800} - 6.02015$
  - $RSF_{432} = 0.0324167 * RSF_{2800} + 0.790833$
  - $RSF_{1296} = 0.010417 * RSF_{2800} - 0.04916$

I have been comparing both methods (at 144 MHz) and the results are quite close. This table gives the RSF_{144} as from the RSF_{2800} :

RSF_{2800} [sfu]	*EME Calculator*	*Polynomial curve*
98	6.00	6.25
107	6.00	7.02
160	10.00	10.29
219	12.00	11.45

Table 4 : Comparison of Radio Solar Flux extrapolation methods

If we assume the antenna is "seeing" the whole sun (which is probably always the case at 144 MHz but not at microwaves, where antenna beamwidths can be very narrow), we are now able to calculate the noise contribution (antenna noise temperature) due to the sun, through the $T_{ant\,sun}$ which is given by [14] :

$$T_{ant\,sun} = \frac{RSF_{144} * 10^{-22} * G_{ant} * \lambda^2}{8 * \pi * k}$$

RSF_{144} : Radio Solar Flux at 144 MHz [sfu]
k : Boltzmann constant, $1.381*10^{-23}$ [J/K]
G_{ant} : antenna gain, relative to isotropic, in ratio [ ]
λ : wavelength [m] = 300/frequency [MHz]

If we take the case of RSF_{2800} being 107 and using the polynomial curve method (RSF_{144} equals 7.02), we find :

$$T_{ant\,sun} = \frac{7.02 * 10^{-22} * 42.66 * \left(\frac{300}{144}\right)^2}{8 * \pi * 1.381 * 10^{-23}} = 374.48 \text{ K}$$

In a similar way as in section 5.4.2., we calculate :

$$T_{ant\,sun\,corrected} = \frac{T_{ant\,sun}}{1.25} + 72.5 = \frac{374.48}{1.25} + 72.5 = 372.1 \text{ K}$$

We pose : $n_{bgd} = k * \left(T_{ant\,bgd\,corrected} + T_{RX}\right) * B$ as the noise power generated (in W/Hz) by the RX connected to the antenna line. N_{bgd} is the same in dBW/Hz.

And : $n_{sun} = k * \left(T_{ant\,sun\,corrected} + T_{ant\,bgd\,corrected} + T_{RX}\right) * B$ as the noise power generated (in W/Hz) by the RX connected to the antenna line when the sun is present in the antenna beamwidth. N_{sun} is the same in dBW/Hz.

Then :

$$NR_{sun} = N_{sun} - N_{bgd} = 10 * \log\left(\frac{n_{sun}}{n_{bgd}}\right) = 10 * \log\left(\frac{T_{ant\,sun\,corrected} + T_{ant\,bgd\,corrected} + T_{RX}}{T_{ant\,bgd\,corrected} + T_{RX}}\right)$$

This equation provides the noise rise (in dB) that should occur on the audio analyser due to the presence of the sun in the antenna beamwidth. However, all this above is true without the influence of the ground (elevated antenna) but, as seen previously, the ground will actually introduce maxima and nulls in the elevation radiation pattern of the antenna. So, if we subtract the calculated sun noise rise (NR_{sun}) of the measured one, which we call "$NR_{measured}$", measured on the audio analyser at a ground reflection maximum, we then have :

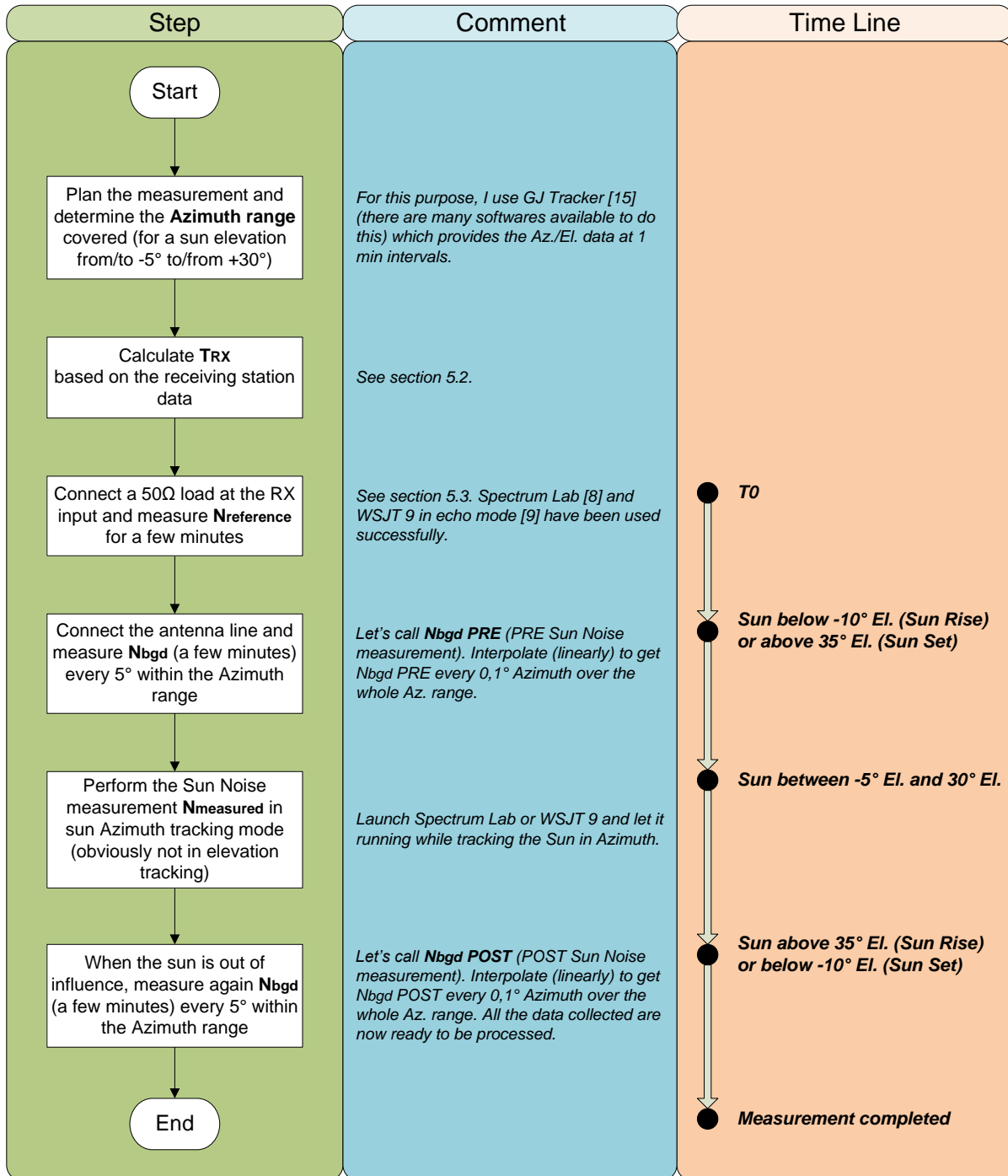$$NR_{measured} = N_{measured} - N_{bgd}$$

And the magnitude of the Ground Gain (GG) in dB is :

$$GG = NR_{measured} - NR_{sun} = \left(N_{measured} - N_{bgd}\right) - \left(N_{sun} - N_{bgd}\right) = N_{measured} - N_{sun}$$

5.5. Measurement steps flow

Fig. 26 provides explanations of the measurement steps to be performed for collecting the data which, after having been processed, will finally give us the magnitude of the Ground Gain.

Step	Comment	Time Line
Start		
Plan the measurement and determine the **Azimuth range** covered (for a sun elevation from/to -5° to/from +30°)	*For this purpose, I use GJ Tracker [15] (there are many softwares available to do this) which provides the Az./El. data at 1 min intervals.*	
Calculate **T_{RX}** based on the receiving station data	*See section 5.2.*	
Connect a 50Ω load at the RX input and measure **N_{reference}** for a few minutes	*See section 5.3. Spectrum Lab [8] and WSJT 9 in echo mode [9] have been used successfully.*	● *T0*
Connect the antenna line and measure **N_{bgd}** (a few minutes) every 5° within the Azimuth range	*Let's call **N_{bgd} PRE** (PRE Sun Noise measurement). Interpolate (linearly) to get Nbgd PRE every 0,1° Azimuth over the whole Az. range.*	● *Sun below -10° El. (Sun Rise) or above 35° El. (Sun Set)*
Perform the Sun Noise measurement **N_{measured}** in sun Azimuth tracking mode (obviously not in elevation tracking)	*Launch Spectrum Lab or WSJT 9 and let it running while tracking the Sun in Azimuth.*	● *Sun between -5° El. and 30° El.*
When the sun is out of influence, measure again **N_{bgd}** (a few minutes) every 5° within the Azimuth range	*Let's call **N_{bgd} POST** (POST Sun Noise measurement). Interpolate (linearly) to get Nbgd POST every 0,1° Azimuth over the whole Az. range. All the data collected are now ready to be processed.*	● *Sun above 35° El. (Sun Rise) or below -10° El. (Sun Set)*
End		● *Measurement completed*

Fig. 26 : Flow diagram for Ground Gain measurement

Detailing every single processing step is beyond the scope of the present article. However, the calculation processing spreadsheet in MS Excel 2007 (Ground Gain Sun Noise Measurement Processing File.xlsm) is available for download on my website [7].

5.6. Measurement campaign results through a case study

This section provides the graphical result of a measurement campaign realized at my station at sun rise and sun set on April 2nd, 2011 (RSF$_{2800}$ = 107). The surroundings are not identical all 360° around ; towards the East (sun rise), the ground is fairly sloping and fairly cluttered, while towards the West (sun set), it is less sloping and slightly cluttered. Several such measurements have been performed and led to the same conclusions ; the example shown here is a typical one.

The measurement setup is the same as described in sections 5.2. and 5.3.

A few words of explanation are needed to understand the graphs that follow (see Fig. 27 to 30).

Fig. 27 and Fig. 29 show the outcome of the measurement in dB relative to N$_{reference}$ (the noise generated by a 50Ω load at room temperature).

The curves shown are :

- NR$_{bgd}$ PRE (red) : the averaged noise rise (in dB) when replacing the 50Ω load by the antenna line **before** the sun noise tracking measurement. The variation with azimuth seen on Fig. 27 and 29 is due to the background noise, considering the sky noise doesn't vary much over the considered azimuth and measurement time span (see section 5.4.2.)
- NR$_{sun}$ PRE (purple) : this is the calculated value (in dB) of the noise increase that should be generated by the sun, on top of the background noise **NR$_{bgd}$ PRE**, without ground influence (see section 5.4.3.)
- NR$_{bgd}$ POST (orange dashed) : like NR$_{bgd}$ PRE but **after** the sun noise tracking measurement
- NR$_{sun}$ POST (green dashed) : like NR$_{sun}$ PRE but on top of the background noise **NR$_{bgd}$ POST**
- NR$_{measured}$ (blue) : the measured noise rise (in dB) during the sun noise tracking measurement, i.e. including both the background noise and the sun noise with ground enhancement

From this data, Fig. 28 and Fig. 30 extract the absolute magnitude of the Ground Gain in dB.

When looking at the graphs, we see that the background noise (and hence also the calculated noise rise due to the sun) is varying during the sun noise tracking measurement. This implies that the magnitude of the measured Ground Gain is actually ranging (measurement uncertainties) between two limits ("GG PRE" and "GG POST") instead of being a single measured figure. In practice, the Ground Gain amount is obviously a single steady figure but the measurement constraints don't allow us to firmly determine it.

- GG PRE (light blue) : the magnitude of the Ground Gain (in dB) based on the background noise (NR$_{bgd}$ PRE) **before** the sun noise tracking measurement
- GG POST (brown) : like GG PRE but **after** the sun noise tracking measurement
- Theoretical Ground Gain pattern over a perfectly reflective flat ground (purple dashed) : self-explanatory, taking into account the radiation pattern of the antenna (here the 12-element DK7ZB at 17m agl)
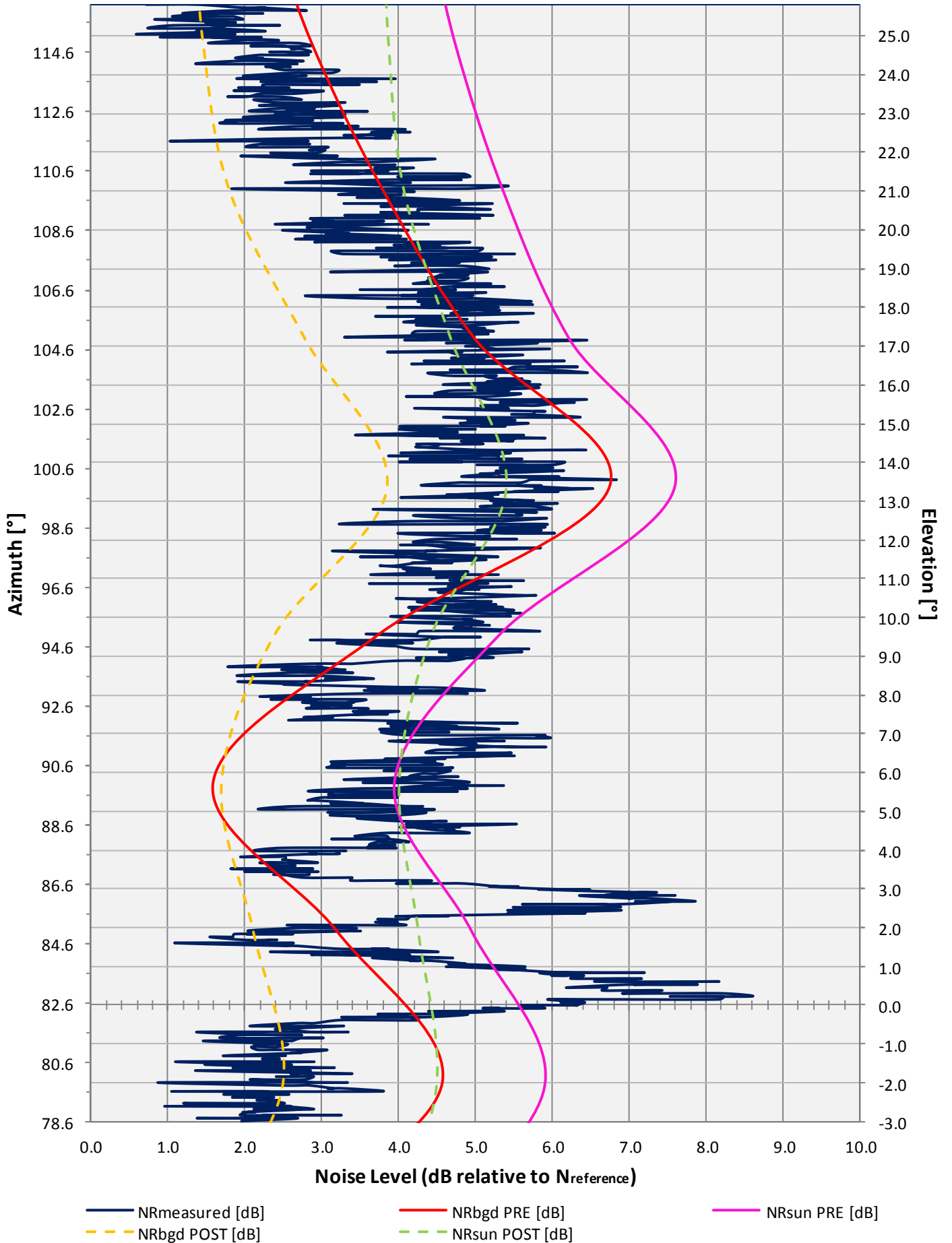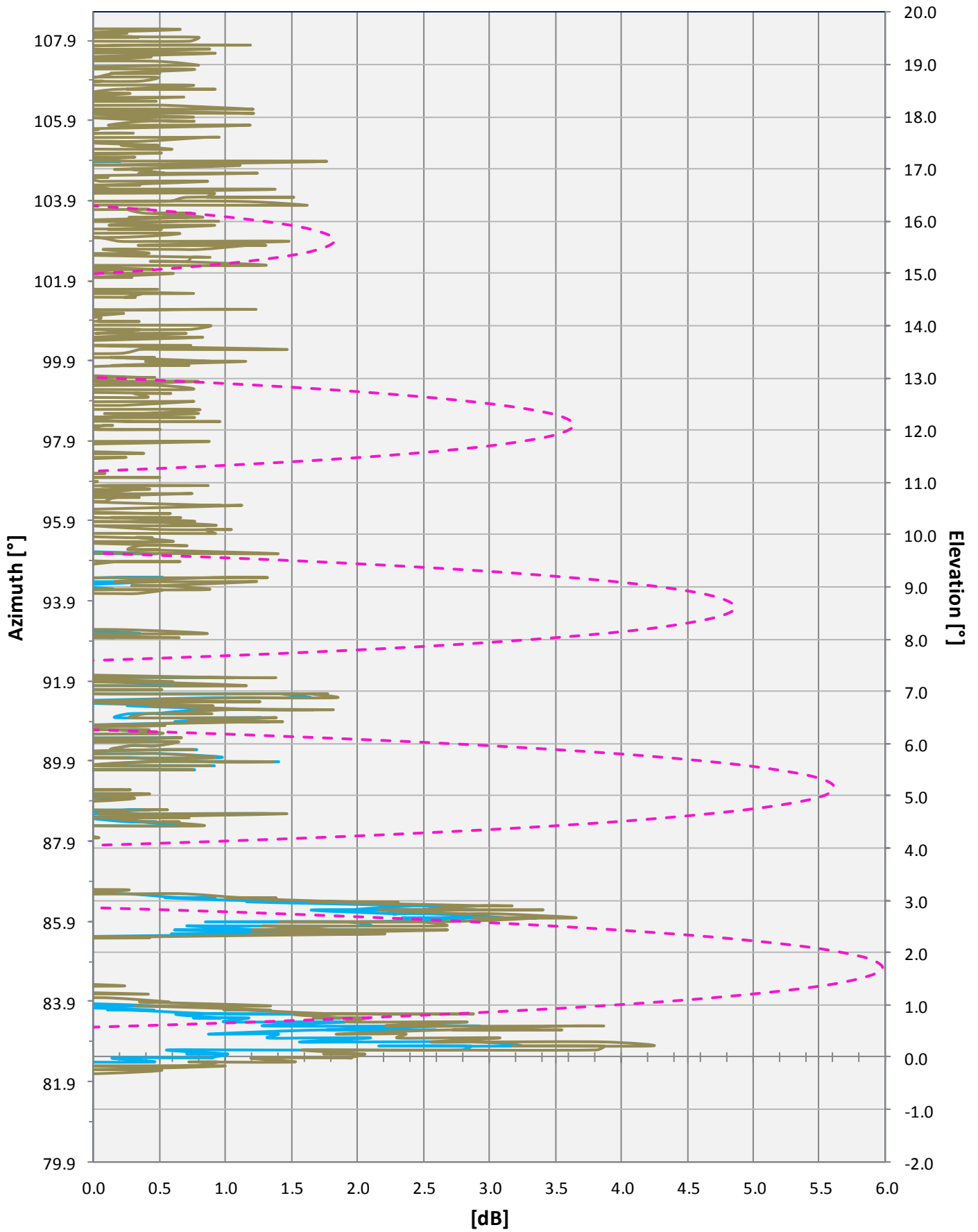
Fig. 27 : Sun rise measurement

Fig. 28 : Ground Gain at sun rise
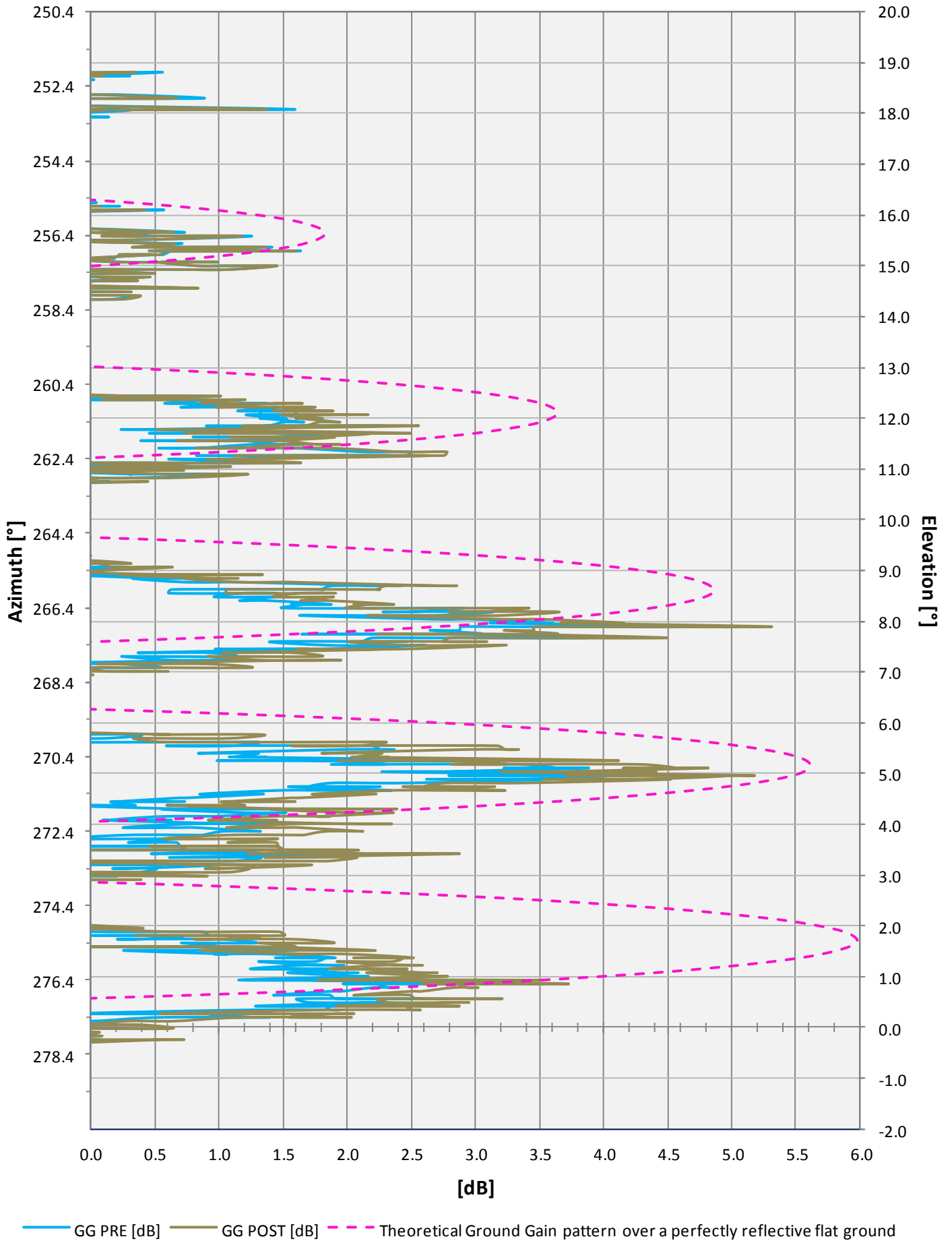
Fig. 29 : Sun set measurement
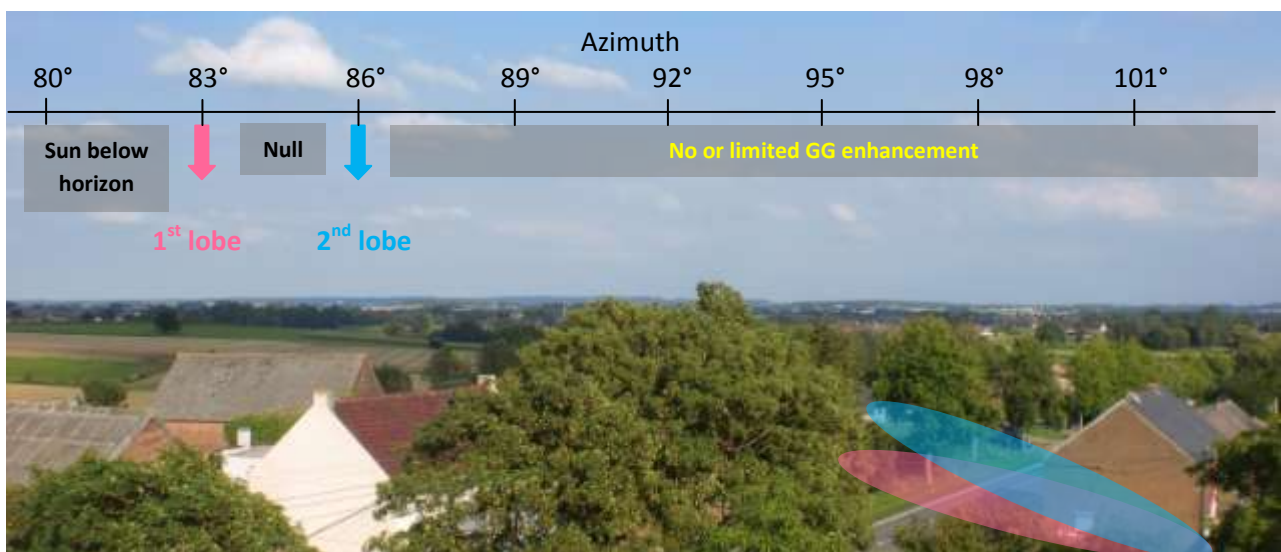
Fig. 30 : Ground Gain at sun set

From the graphs (Fig. 27 to 30), the conclusions to be drawn are quite straightforward.

- **Sun rise** :
    - Fig. 31 and Fig. 32 show the associated terrain and clutter
    - Two significant lobes at 0.5° and 2.8° elevation ; at higher elevations, the measurement is either too noisy or there is no or very limited Ground Gain enhancement
    - 3 dB in average of Ground Gain enhancement for the two lobes
    - The elevation angles are well lower than the theoretical ones. This is due to the sloping ground in front of the antenna in these azimuths, as explained before (section 4.5.)
    - Not surprisingly, the two lobes build between houses (in red on Fig. 31), but where the terrain is cluttered with houses in the area where the lobe should be building, there is no noticeable (or very limited) Ground Gain enhancement
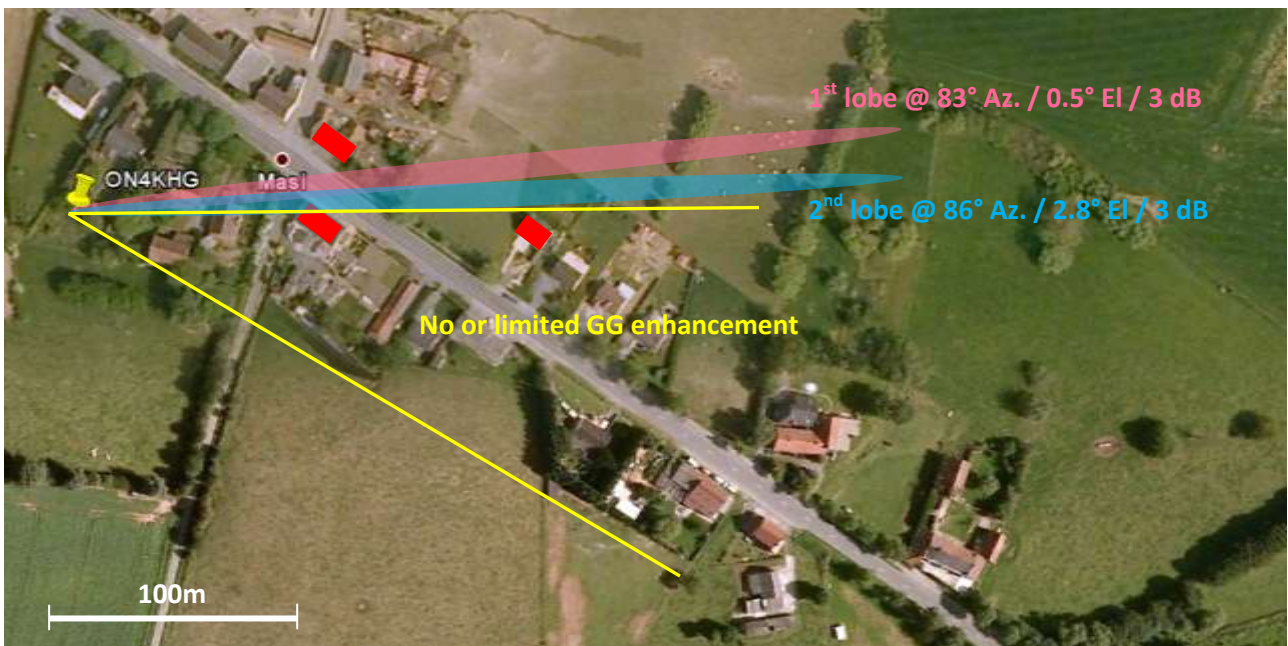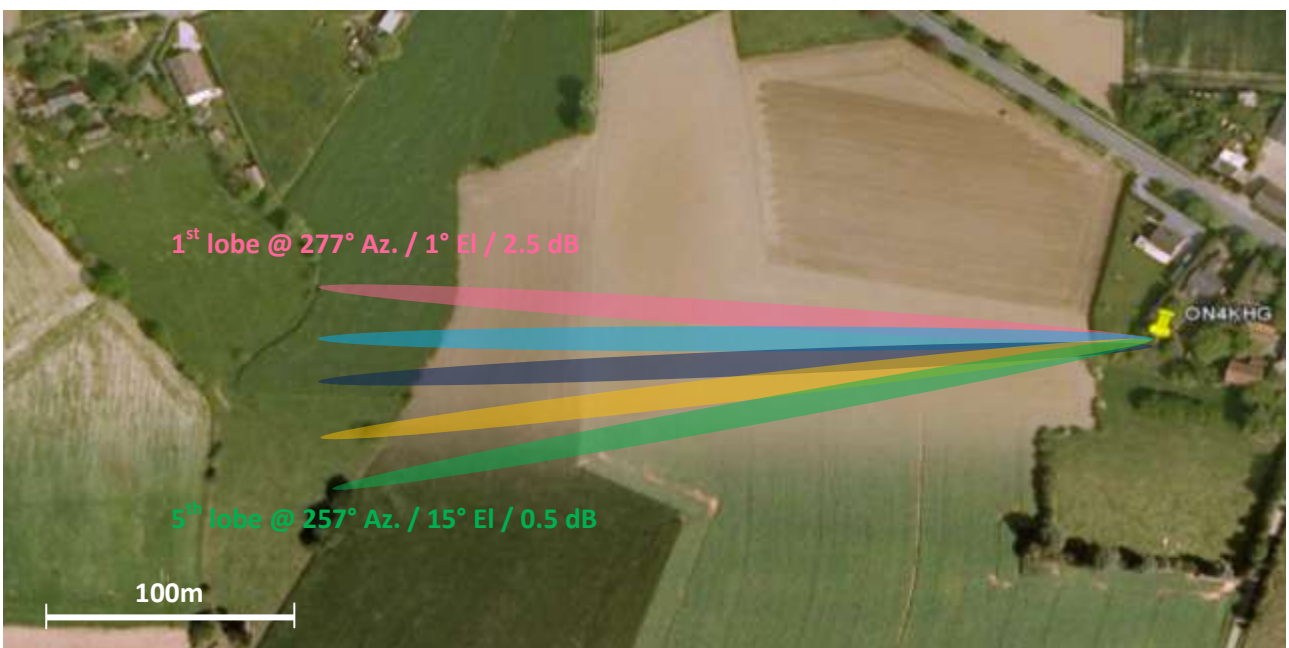

**Fig. 31 : Elevated view of the terrain at sun rise**

Fig. 32 : Horizon at sun rise

- **Sun set :**
  - Fig. 33 and Fig. 34 show the associated terrain and clutter
  - Five distinctive Ground Gain lobes at 1°, 5°, 8°, 11.5° and 15.4° elevation
  - Up to 4.5 dB enhancement for the second and third lobes ; 2.5 dB for the first and fourth lobes (the fourth lobe is due to the antenna radiation pattern)
  - The first lobe exhibits less Ground Gain enhancement than one would have expected. With the antenna at 17m agl, this lobe builds between 98m and 3348m from the antenna (theoretical figures over flat ground) but in this direction there are big farms at 800m, 1.1km and 1.2km. Although these are too distant to be visible in Fig. 33 and Fig. 34, they do seem to affect the formation of the first lobe. However, at the closer ranges, where the second and third lobes are building, there are only open fields and Ground Gain enhancement is in fact observed
  - The elevation angles are a bit lower than the theoretical ones, again because of the slightly sloping ground (less tilted than in the sun rise direction)

Fig. 33 : Elevated view of the terrain at sun set
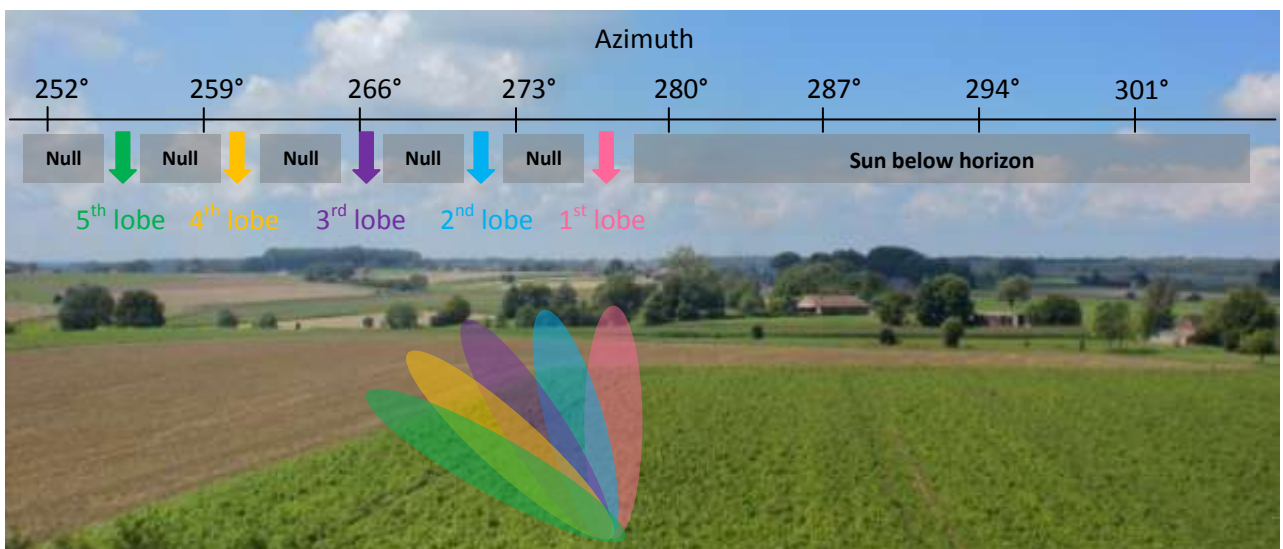
Fig. 34 : Horizon at sun set

5.7. Accuracy and applicability

The measurement method described here is not new ; it is broadly inspired from the well known Y-factor method used to determine the G/T figure of merit of receiving stations. This method compares a "hot" noise source (e.g. the sun) with a "cold" one (e.g. a low noise part of the sky) and to derive the Y-factor. The larger the difference in noise power density (or noise temperature) between the two sources, the better the accuracy.

Here, if we assume the background noise (N_{bgd}) to be the cold source and the sun (N_{sun}) to be the hot one, we see on the graphs of the preceding section that if the calculated noise rise due to the sun amounts to 2.5 dB at best when the background noise level is low, it can be down to 0.5 dB when the background noise is high. This provides a limited accuracy in highly noisy environments. Moreover, the background noise is varying during the whole measurement time span ; it is likely to be due to the human activities (man-made noise) and can't be controlled. But also, variations of the gain of the whole receiving setup can lead to the same apparent effect. I once measured the gain of the setup loaded on a 50Ω load over a 12-hour period, and it fluctuated by 1.5 dB. This makes another source of inaccuracy, along with the possible variation in preamplifier (in front of the Transceiver or inside the Transverter) gain when changing between the 50Ω load and a slightly mismatched antenna [16].

As stated in [10] and [12], the accuracy of the extrapolated Radio Solar Flux (RSF) is also very questionable.

Though this paper focuses on 144 MHz, one can ask about the applicability on 50 MHz. The answer is that though a Ground Gain enhancement (if any) is actually present, it is almost impossible to accurately measure its magnitude because the RSF at 50 MHz is lower than at 144 MHz and the background noise (at least the galactic noise) is higher.

At any given location, the span of azimuth ranges over which the Ground Gain can be measured is determined by the latitude. Here, at 50° 36' North, the sun rises between the azimuths 50° and 128° and sets between 231° and 309°. This makes less than half the full 360° compass. More northern locations will experience broader spans and southern locations narrower.

6. Conclusion

Primarily driven by the wish to understand to what extend ground reflections can enhance successful EME communications on 144 MHz, this "study" actually goes a step further, by highlighting how the environment surrounding an antenna system pointing to the horizon can affect the performance of an amateur radio station. In other words, but only under certain circumstances and all other things being equal, a careful choice of site location can render a station up to 6 dB more powerful (in transmission and reception) over flat land than another one. In particular environments, this advantage can even be higher if more than two paths to/from the antenna are involved.

Not only can this Ground Gain improvement make a single-Yagi station perform like a multi-Yagi one on its first radiation pattern lobe (the one elevated least above the horizon, depending on the

antenna height) in the elevation plane, but it will assist with the higher elevation lobes too, which an actual multi-Yagi (e.g. two stacked, two bayed) antenna system doesn't allow (or very much less) !

Although the first elevation lobe is the most important for the troposcatter traffic, the enhanced upper lobes may be quite helpful for meteor-scatter, (chordal) Es, to enter a tropo duct and of course for EME operation without antenna elevation capability.

One outcome of this analysis is the conclusion that placing an antenna as high as possible up in the air is not always an absolute requirement. Indeed, the higher an antenna, the further away from it the Ground Gain lobes will build and, at some sites, the higher the likelihood that the ground is cluttered with vegetation and/or buildings (attenuating the magnitude of the reflected wave). In this case, is it worth losing 6 dB of Ground Gain by winning a few (tens) kilometres of short-range radio horizon ? All is a matter of trade-off.

We have learnt that the maximum magnitude of elevation lobes for horizontal polarization can occur in nulls of vertical one and vice versa, so using dual polarization (H-V) antennas for EME operation can obviously bring some benefit. And this is without even speaking of the advantages of H-V antennas regarding the ionospheric effects (Faraday polarization rotation).

It has also been demonstrated here that the ground flatness (with respect to the wavelength) is of the prime importance to achieve a good Ground Gain, and that the horizontal polarization will usually experience more Ground Gain than the vertical one. As far as the first elevation lobe is concerned, we have seen that the nature of the soil is not an important parameter for horizontal polarization, and that even poorly conductive ground can provide a very similar Ground Gain enhancement as sea water. The main difference being that a takeoff over water is far less likely to be spoiled by local clutter (vegetation and/or buildings). But do note that the conclusions for vertical polarization are completely different.

Finally, the Ground Gain measurement method described here, though not revolutionary and of limited applicability, will allow everybody to make his own idea on how the environment is acting on the performance of his radio station.

7. References

[1a] : "Ground gain and radiation angle at VHF", by Palle Preben-Hansen, OZ1RH, http://www.qsl.net/oz1rh/gndgain/gnd_gain_eme_2002.htm

[1b] : "Precedings of the IRE – Scatter Propagation Issue", volume 43, number 10 of October 1955

[2] : http://hamsoft.ca/pages/mmana-gal.php

[3] : http://home.ict.nl/~arivoors

[4] : "A general model for VHF aeronautical multipath propagation channel", Aeronautical Mobile Communications Panel (AMCP), Working Group, Honolulu, Hawaii, 19-28 January 1999, Presented by Arnaud Dedryvere, http://www.icao.int/anb/panels/acp/wg/d/WGD10/wgd10_06.pdf

[5] : "Earth Constants", TAI Inc. Consuletter International, Vol. 6, N° 5, by Peter N Saveskie

[6] : "Evaluation of ray-tracing in wideband characterization of microcellular propagation", Helsinki University of Technology, 18/10/2001, by Annemarie Hjelt

[7] : http://www.on4khg.be/EME_Gr_Gain.html

[8] : http://www.qsl.net/dl4yhf/spectra1.html

[9] : http://www.physics.princeton.edu/pulsar/K1JT/wsjt.html

[10] : "Sun Noise – Solar Flux Measurements", GippsTech 2008, by Doug Mc Arthur, VK3UM, http://www.vk3um.com/Documents/SunNoise_Measurements.pdf

[11] : http://www.swpc.noaa.gov/ftpdir/lists/radio/rad.txt

[12] : http://vk3um.com

[13] : "Performance evaluation for EME-systems", DUBUS 3/1992, by Rainer Bertelsmeier, DJ9BV and Patrick Magnin, F6HYE, http://dpmc.unige.ch/dubus/9203-3.pdf

[14] : "Antenna calibration using the 10.7cm Solar Flux", Dominion Radio Astrophysical Observatory, Pencticton, Canada, by Ken Tapping, http://www.k5so.com/RadCal_Paper.pdf

[15] : http://www.bigskyspaces.com/w7gj

[16] : "Myths and Facts about Preamp. Tuning", by Rainer Bertelsmeier, DJ9BV, in DUBUS Technik V